HOKKAIDO UNIVERSITY

Title	A single mutation converts Alr5027 from cyanobacteria Nostoc sp. PCC 7120 to a heme-binding protein with heme-degrading ability
Author(s)	Dojun, Nobuhiko; Muranishi, Kazuyoshi; Ishimori, Koichiro; Uchida, Takeshi
Citation	Journal of Inorganic Biochemistry, 203, 110916 https://doi.org/10.1016/j.jinorgbio.2019.110916
Issue Date	2020-02
Doc URL	http://hdl.handle.net/2115/83251
Rights	©2019, Elsevier. Licensed under the Creative Commons Attribution-NonCommercial-NoDerivatives 4.0 International http://creativecommons.org/licenses/by-nc-nd/4.0/
Rights(URL)	http://creativecommons.org/licenses/by-nc-nd/4.0/
Type	article (author version)
File Information	j.jinorgbio.2019.110916-HUSCAP.pdf

Instructions for use

Hokkaido University Collection of Scholarly and Academic Papers : HUSCAP

A single mutation converts Alr5027 from cyanobacteria *Nostoc* sp. PCC 7120 to a heme-binding protein with heme-degrading ability

Nobuhiko Dojun[a], Kazuyoshi Muranishi[a], Koichiro Ishimori[a.b], and Takeshi Uchida[a,b,*]

[a] Graduate School of Chemical Sciences and Engineering, Hokkaido University, Sapporo 060-8628, Japan

[b] Department of Chemistry, Faculty of Science, Hokkaido University, Sapporo 060-0810, Japan

*Corresponding author at Department of Chemistry, Faculty of Science, Hokkaido University, Sapporo 060-0810, Japan.

E-mail address: uchida@sci.hokudai.ac.jp, Phone: +81-11-706-3501 (T. Uchida).

Keywords: cyanobacteria, *Vibrio cholerae*, heme oxygenase, redox protein, enzyme, heme

ABSTRACT

HutZ from *Vibrio cholerae* (*Vc*HutZ) is a dimeric protein that catalyzes oxygen-dependent degradation of heme. The reaction mechanism is the same as that of canonical heme oxygenase (HO), but the structure of HutZ is quite different from that of HO. Thus, we postulate that HutZ has evolved via a different pathway from that of HO. Alr5027 from cyanobacteria possessing proteins potentially related to ancestral proteins utilizing O_2 in enzymatic reactions is homologous to HutZ family proteins (67% similarity), but the heme axial ligand of HutZ is not conserved in Alr5027. To investigate whether Alr5027 can bind and degrade heme, we expressed Alr5027 in *Escherichia coli* and purified it. Although Alr5027 did not bind heme, replacement of Lys164, corresponding to the heme axial ligand of HutZ, with histidine conferred heme-binding capability. The K164H mutant produced verdoheme in the reaction with H_2O_2, indicating acquisition of heme-degradation ability. Among the mutants, the K164H mutant produced verdoheme most efficiently. Although the K164H mutant did not degrade heme through ascorbic acid, biliverdin, the final product of *Vc*HutZ, was formed by treatment of verdoheme with ascorbic acid. An analysis of Trp103 fluorescence indicated elongation of the distance between protomers in this mutant compared with *Vc*HutZ—the probable cause of the inefficiency of ascorbic acid-supported heme-degradation activity. Collectively, our findings indicate that a single lysine-to-histidine mutation converted Alr5027 to a heme-binding protein that can form verdoheme through H_2O_2, suggesting that HutZ family proteins have acquired the heme-degradation function through molecular evolution from an ancestor protein of Alr5027.

1. Introduction

Heme oxygenase (HO) is an enzyme that catalyzes stereospecific cleavage of heme to produce biliverdin, Fe^{2+}, and carbon monoxide (CO) [1–3]. Animals utilize the heme-degradation products, biliverdin and CO, as antioxidant and gaseous signaling molecules, respectively [4,5]. In higher plants, algae and cyanobacteria, HO synthesizes bilin pigments, a group of open tetrapyrroles, for photosynthetic antennae [6]. Most pathogenic bacteria also possess HO homologues that liberate iron from host-derived heme for use as a cofactor by other proteins [7,8]. Because these bacteria use heme as an iron source, it has been postulated that pathogenic bacteria have evolved these heme-degrading enzymes for survival [9–11]. The structures of bacterial HOs from *Corynebacterium diphtheria* [12], *Neisseria meningitides* [13], and *Pseudomonas aeruginosa* [14] consist of a monomer with an all α-helical fold, a structural feature quite similar to that of eukaryotic HOs [15]. The reaction mechanism of bacterial HOs is also the same as that of eukaryotic HOs [16]. The noncanonical HO-type enzymes, IsdG and IsdI, from *Staphylococcus aureus* were recently identified and shown to adopt a ferredoxin-like α/β-sandwich fold [17] and possess a unique heme-degradation mechanism. These enzymes convert heme to staphylobilin with release of *meso*-carbon as formaldehyde, but not CO [18,19].

A new family of heme-degrading proteins that lack homology to previously described HOs was recently discovered in *Campylobacter jejuni* (ChuZ) [20], *Helicobacter pylori* (HugZ) [21], and *Vibrio cholerae* (HutZ) [22,23]. ChuZ and HugZ form homodimers with a split β-barrel, a structure distinct from that of canonical HOs. We found that *V. cholerae* HutZ, which is homologous to HugZ, degrades heme in a pH-dependent manner: when ascorbic acid is used as an electron source, it is inactive at pH 8.0, but is active at pH 6.0 [22]. We discovered that the intermediates of the heme-degradation reaction by HutZ are the same as those observed in the reaction catalyzed by the canonical HOs (Fig. S1) [16,24–26]. However, a structural analysis of HugZ, a homologous protein from *H. pylori*, revealed that HutZ has no

sequence or structural similarity to HOs (Fig. S2) [21]. These observations indicate that HutZ has evolved from a different ancestor than canonical HOs.

To search for an ancestral protein of HutZ, we focused on cyanobacteria, which evolved ~2.7 billion years ago from ancient phototrophic organisms that previously inhabited Earth [27]. These ancient organisms had evolved two photosystems, namely the high-potential water-oxidizing photosystem II and the low-potential ferredoxin-reducing photosystem I, resulting in oxygenic photosynthesis. This most decisive evolutionary step marked a turning point in evolution on Earth, opening up the era of an aerobic, oxygen-containing biosphere and atmosphere. Recent evidence suggests that as O_2 molecules became integral to biochemical pathways, many enzymatic reactions central to anoxic metabolism were effectively replaced in aerobic organisms [28]. Thus, we hypothesized that cyanobacteria, which utilize O_2 molecules in their enzymatic reactions, would have proteins related to ancestral proteins for O_2 metabolism. We searched for HutZ homolog proteins from cyanobacteria *Nostoc* sp. PCC7120. A BLAST (http://blast.ncbi.nlm.nih.gov/Blast.cgi) search revealed that the sequence of Alr5027, a protein of unknown function [29], is highly similar to *V. cholerae* HutZ (*Vc*HutZ) (43% identity and 67% similarity) [30]. Arg92, His170, and Asp132 in *Vc*HutZ are key residues in the heme-degradation reaction (Fig. S3) [22,31]. Arg92, which is located in the distal site of heme, acts as a hydrogen-bond donor for iron-bound O_2 [21,22]. His170 is a heme axial ligand, which forms a hydrogen bond with Asp132 that retains heme in an appropriate position for degradation[31]. Although Arg92 and Asp132 of *Vc*HutZ, corresponding to Arg86 and Asp126 of Alr5027, respectively, are conserved in Alr5027, His170 of *Vc*HutZ is not conserved (the corresponding residue in Alr5027 is Lys164) (Fig. 1A). A phylogenetic tree was constructed on the basis of a multiple sequence alignment of the HugZ family by applying the maximum likelihood method using MEGA 7 [32] (https://www.megasoftware.net/) (Fig. 1B). This analysis indicated that Alr5027 is situated at a branch that is separate from other members of the HugZ family. These findings

led us to predict that members of the HutZ family share a common ancestor protein with Alr5027. However, whether Alr5027 is capable of binding and degrading heme was unknown. The purpose of this study is to confirm whether Alr5027 can obtain heme-degrading ability by introducing some mutations, which would mimic molecular evolution of the HutZ family.

In this study, we expressed Alr5027 in *Escherichia coli* and examined its heme-binding and heme-degradation properties. Alr5027 did not bind to heme, reflecting the absence of a conserved, putative heme ligand. Replacement of lysine at position 164 with histidine (K164H) rendered the protein capable of binding to heme. When H_2O_2 was used as an electron source, verdoheme, an intermediate involved in heme degradation by HO, was produced. Our results show that the single replacement of Lys164 with histidine converted Alr5027 to a heme-binding protein with the ability to form verdoheme. These findings suggest that members of the HutZ family have acquired their heme-degradation function through molecular evolution from a common ancestor of *Vc*HutZ and Alr5027.

2. Materials and Methods

2.1. Materials

The chemicals used in this study were purchased from Wako Pure Chemical Industries (Osaka, Japan), Nacalai Tesque (Kyoto, Japan) or Sigma-Aldrich (St. Louis, MO), and were used without further purification.

2.2. Expression and purification of Alr5027

The *alr5027* gene, with codons optimized for *E. coli* expression (Eurofins Genomics, Tokyo, Japan), was amplified by polymerase chain reaction (PCR) and cloned into a modified pET-28b vector [33]. The expression plasmid was transformed into the *E. coli* BL21(DE3) strain (Nippon Gene, Japan) and cultured at 37 °C in LB broth supplemented with 50 μg mL^{-1} kanamycin. After the optical density at 600 nm (OD_{600}) reached 0.8, expression of the His_6-tagged protein was induced with 0.4 mM isopropyl β-$_D$-thiogalactopyranoside. The cells

were further grown at 20 °C overnight and harvested by centrifugation. The cell pellet was suspended in lysis buffer containing 50 mM Tris-HCl, 500 mM NaCl (pH 8.0), 1.0% Nonidet P-40, 1 mg mL^{-1} lysozyme and DNase, and incubated on ice for 60 min. The sample was centrifuged at 18,000 rpm for 30 min, and the supernatant was mixed with 5.0 mL of Ni-NTA agarose (Nacalai Tesque, Japan) with gentle agitation for 1 h at 4 °C. The slurry was poured into a column and washed with lysis buffer supplemented with 20 mM imidazole (25 mL), after which the protein was eluted with elution buffer (50 mM Tris-HCl, 500 mM NaCl, 250 mM imidazole, pH 8.0). Eluted Alr5027 was incubated with Turbo 3C protease (Accelagen, San Diego, CA, USA) for ~16 h at 4 °C to cleave the His_6-tag. After cleavage, the reaction mixture was re-applied to the Ni-NTA resin, and the flow-through fraction was collected. Tag-cleaved Alr5027 was then applied to a HiLoad 16/600 Superdex 200 gel-filtration column (GE Healthcare, Uppsala, Sweden) pre-equilibrated with 50 mM Tris-HCl and 150 mM NaCl (pH 8.0). Protein purity, assessed by sodium dodecyl sulfate-polyacrylamide gel electrophoresis (SDS-PAGE) on 12.5% polyacrylamide gels, was determined to be ~95%.

Mutations were introduced using a PrimeSTAR mutagenesis basal kit from Takara Bio (Otsu, Japan). Primers used for construction of the clone and mutagenesis are shown in Supplementary Table S1.

2.3. Measurement of heme binding to Alr5027

Heme binding was tracked by difference spectroscopy in the Soret region of the UV-visible spectrum. Successive aliquots of 0.5 mM hemin in 0.1 M NaOH were added to both the sample cuvette containing 10 μM Alr5027 and reference cuvette containing buffer only. Spectra were recorded 3 min after the addition of each heme aliquot. The absorbance difference at 414 or 415 nm was plotted as a function of heme concentration, and the dissociation constant ($K_{d,heme}$) was calculated using the quadratic binding equation (equation 1):

$$\Delta A = \Delta A_{\max} \frac{[\mathrm{P}]+[\mathrm{H}]+K_{\mathrm{d,heme}} - \sqrt{([\mathrm{P}]+[\mathrm{H}]+K_{\mathrm{d,heme}})^2 - 4[\mathrm{P}][\mathrm{H}]}}{2[\mathrm{P}]}, \quad (1)$$

where [P] and [H] represent the total protein and hemin concentrations, respectively; ΔA is the change in absorption difference between the sample and reference cell upon addition of hemin; and $\Delta A_{\max}$ is the maximum of the absorption difference upon addition of hemin. The millimolar extinction coefficient was determined using the pyridine hemochrome method [34]. All titrations were repeated in triplicate, and errors are given as the standard deviations.

2.4. Spectroscopy

Optical spectra of purified proteins were recorded with a UV-visible spectrophotometer (V-660; Jasco, Tokyo, Japan) at 25 °C. Fluorescence spectra were recorded using a FP-8500 spectrometer (Jasco). Protein samples were excited at 295 nm to avoid contribution from tyrosine resides. The Alr5027 concentration was 5 μM in 50 mM Tris-HCl and 150 mM NaCl (pH 8.0). The distance (r) between tryptophan and heme was estimated from the efficiency (E) of Förster energy transfer from tryptophan to heme, defined as:

$$E = \frac{R_0^6}{R_0^6 + r^6} \quad (2)$$

where R_0 represents the Förster distance and is 29 Å for heme and tryptophan [35]. The energy transfer efficiency, E, was calculated using the fluorescence intensity of apo-Alr5027 (F_{apo}) and heme-Alr5027 (F_{heme}):

$$E = \frac{F_{\mathrm{apo}} - F_{\mathrm{heme}}}{F_{\mathrm{apo}}} \quad (3)$$

2.5. Heme-degradation activity

The heme-degradation reaction of Alr5027 was monitored by spectrophotometry as described elsewhere [36]. Briefly, 1.9 mL of a hemin-reconstituted protein solution (final concentration,

3.0 μM) in 50 mM Tris-HCl and 150 mM NaCl (pH 8.0) was placed in a cuvette, and the reaction was started by adding 100 μL of 2 mM H_2O_2 or 20 mM ascorbic acid in the same buffer at 25 °C. Spectra were recorded at 1-min intervals for 10 min for H_2O_2 (final concentration, 0.1 mM), and at 2-min intervals for 30 min for ascorbic acid (final concentration, 1 mM). In the case of reactions with ascorbic acid, 1 mg mL^{-1} of bovine liver catalase was added to cause H_2O_2 dismutation. Iron liberated from products by heme-Alr5027 was obtained by adding a saturated solution of HCl (~8 M) to the heme-degradation reaction mixture, resulting in efficient extraction of pigments from the proteins. Solid-phase extraction of the reaction products was performed using a Supelclean LC-18 column (Supelco, Bellefonte, PA, USA). The column-bound sample was washed with 20% (v/v) methanol and 80% (v/v) water, and eluted with methanol. The effluents were analyzed on an LC-2000 HPLC system (Jasco) equipped with a ZORBAX Extend-C18 column (3.0 × 150 mm, 3.5 μm silica; Agilent Technologies, Palo Alto, CA, USA) using a linear gradient from 50% (v/v) methanol and 50% (v/v) 0.1 M ammonium acetate to 80% (v/v) methanol over 60 min at a flow rate of 0.5 mL min^{-1}. The eluent was monitored at 380 nm. Biliverdin dimethyl esters standards were prepared as previously described [37].

2.6. Heme reduction rate

The heme reduction rate, k_{red}, was determined by monitoring changes in absorbance at 418 nm. The ferric heme-Alr5027 complex (10 μM) was reduced with 1 mM ascorbic acid. In addition to an oxygen-scavenging system composed of glucose and glucose oxidase, catalase was added to the solution to maintain anaerobic conditions [38]. The reaction was conducted under a CO atmosphere to prevent heme degradation and/or auto-oxidation by trace levels of contaminating O_2 [39]. The k_{red} was obtained by fitting the time course of changes in absorbance at 418 nm to a single-exponential expression.

3. Results and discussion

3.1. Expression and purification of Alr5027

The *alr5027* gene was expressed in *E. coli* and purified using a His_6-tag affinity column. After cleavage of the His_6-tag and size-exclusion chromatography, only a single band with an apparent molecular mass of approximately 16 kDa was observed on SDS-PAGE gels (Fig. 2A), in agreement with the calculated molecular mass of Alr5027 (18 kDa). An analysis of purified Alr5027 by size-exclusion chromatography indicated that the protein existed as a dimer (40 kDa) (Fig. 2B), as observed for *Vc*HutZ [22] .

3.2. Heme-binding properties of Alr5027

The purified protein showed no absorption in the visible region, indicating that it was purified in a pigment-free form (i.e., without heme) (Fig. 3, red line). Addition of an aliquot of hemin solution to Alr5027 resulted in the appearance of a broad Soret band at ~389 nm (Fig. 3, blue line), which was almost identical to that of free hemin (Fig. 3, black line). To determine whether Alr5027 is capable of binding to heme, we performed a heme-titration experiment. The absorbance difference at 414 nm, obtained by subtracting the spectrum of free hemin at various concentrations, increased only slightly with increasing concentrations of heme (Fig. 3, inset). This result is clearly different from that of a mutant that bound heme as described next, indicating that wild-type (WT) Alr5027 did not bind heme.

3.3. Heme-binding properties of the K164H mutant

A sequence alignment of the HugZ family is shown in Fig. 1A. His170, the heme axial ligand in *Vc*HutZ, is conserved among members of the family except Alr5027. Thus, we predicted that Alr5027 would attain heme-binding ability if histidine were introduced at the corresponding position. To this end, we replaced Lys164 with histidine (Fig. 1C) and purified the resulting K164H mutant using the same procedure as used for WT Alr5027. Following addition of hemin to the mutant, the resultant solution exhibited a Soret band at 413 nm (Fig. 4A, red line), which was almost identical to that of heme-HutZ [22]. The spectrum was

clearly distinguishable from that of WT Alr5027 with hemin (Fig. 4A, black line), suggesting that heme specifically bound to the mutant and forms a hydroxide ion-bound form (Fe^{3+}–OH^-), as observed in *Vc*HutZ [22]. The apparent dissociation constant ($K_{d,heme}$), calculated by fitting the data to equation 1, was determined to be 0.24 ± 0.03 μM, which is approximately 5-fold larger than that reported for *Vc*HutZ (0.052 ± 0.020 μM) [22]. These results show that the replacement of Lys164 with histidine converts Alr5027 into a heme-binding protein.

3.4. Heme-degradation activity of the K164H mutant

Because we found that the K164H mutant binds heme, we next examined whether it also degrades heme. We first used H_2O_2 as an electron source because verdoheme, a key intermediate in the heme-degradation reaction, is formed when heme-bound *Vc*HutZ reacts with H_2O_2 (Fig. S1) [22]. In the reaction of the heme-K164H mutant with H_2O_2, the absorbance at 652 nm increased (Fig. 4B), reaching a value approximately 72% of that for *Vc*HutZ [22]. This band did not appear following treatment of heme-bound WT Alr5027 with H_2O_2 (Fig. 4C). The peak position at 652 nm corresponded to that of the verdoheme of *Vc*HutZ [22,26], indicating that verdoheme was produced in the reaction of the mutant with H_2O_2.

A decrease in the Soret band does not always indicate heme degradation, because reaction intermediates of hemoproteins with H_2O_2 called as compound I ($Fe^{IV}=O^{+\bullet}$), compound ES (Fe^{IV}=O/amino acid radical) and compound II (Fe^{IV}=O) are known to have features of a relatively weak Soret band [40,41]. The reaction of myoglobin with H_2O_2 resulted in a decrease in the intensity of the Soret band (Fig. S4A), but absorption was restored by the addition of *o*-methoxyphenol (guaiacol) (Fig. S4B). To investigate whether the decrease in Soret absorbance in the K164H mutant (Fig. 4B) was reversible, we added guaiacol. The intensity of the Soret band did not change after the addition of guaiacol (Fig. S4C). Collectively, these results indicate that the heme-K164H mutant produced verdoheme, but not compound I or compound II. In most cases, H_2O_2 binds to heme to form compound II and OH

radical, as observed in myoglobin [42–44]. OH radical randomly attacks heme macrocycle and breaks heme. Thus, verdoheme is not formed in most hemoproteins. In the case of the K164H mutant, the enhancement of the 652-nm band during the reaction with H_2O_2 clearly showed the formation of verdoheme, suggesting this mutant obtained a heme-degrading ability by only single mutation.

Heme can be cleaved at any one of four structurally nonidentical *meso* positions, producing four isomers of verdoheme, whose absorption spectra are different from each other [36]. To identify the oxidation site of verdoheme of the K164H mutant, we added pyridine to the reaction solution, which resulted in a visible band at 660 nm typical of pyridine-verdohemochrome [37] (Fig. S5A). The absorption maximum of verdohemochrome of the K164H mutant (660 nm) was close to that of β-verdoheme (663 nm) and δ-verdoheme 660 nm), but not to that of α-verdoheme (680 nm) or γ-verdoheme (648 nm) [37], suggesting that the β- or δ-*meso* position was cleaved in the reaction of the K164H mutant with H_2O_2, as observed for *Vc*HutZ [22].

To demonstrate the catalytic activity of the K164H mutant, we also examined the heme-degradation reaction of the heme-K164H mutant using ascorbic acid as an electron source. The reaction was conducted in the presence of the H_2O_2-scavenger catalase. Spectral changes following addition of ascorbic acid at pH 8.0 are shown in Fig. 5A. The Soret band showed very little decrease, and no clear band appeared in the 500–800 nm region, suggesting that no heme-degradation occurred under these conditions [45]. As reported previously [22], the heme-degradation reaction of heme-*Vc*HutZ with ascorbic acid is significantly accelerated at pH 6.0. However, lowering the pH from 8.0 to 6.0 did not promote a decrease in the Soret band, indicating that heme in the K164H mutant was not degraded in the reaction with ascorbic acid (Fig. 5B).

3.5. Heme-binding properties and degradation ability of D163H and G165H mutants

As described above, the K164H mutant bound to heme and converted it to verdoheme

using H_2O_2, whereas it did not degrade heme in the reaction with ascorbic acid, despite possessing a proximal histidine at position 164. We postulated that the position of the proximal histidine is not appropriate for heme degradation. Thus, to shift the position of histidine, we replaced Asp163 or Gly165 with histidine. The sequence of mutants in the C-terminal region (163–165) is shown in Fig. 1C. The absorption spectrum of the D163H mutant in the presence of heme was similar to that of WT Alr5027 (Fig. 6A), suggesting that heme did not bind to the histidine at position 163. In contrast, addition of heme to the G165H mutant resulted in the appearance of a Soret band at 414 nm (Fig. 6B), indicating that this mutant specifically bound to heme. The $K_{d,heme}$ value was 0.44 ± 0.06 μM, which is similar to that of the K164H mutant (0.24 ± 0.03 μM). Thus, the introduced histidine at position 165 also coordinates with heme.

Next, we conducted the heme-degradation reaction for the heme-G165H mutant using H_2O_2 as an electron donor. A small band from verdoheme appeared at 653 nm following addition of H_2O_2 to the heme-G165H mutant (Fig. 6C). This behavior of the heme-G165H mutant was quite similar to that of the heme-K164H mutant, but the amount of verdoheme was smaller—approximately 34% that of *Vc*HutZ (Fig. 4B).

In addition, we prepared the G165HG mutant, in which histidine was inserted between Lys164 and Gly165 to avoid placing histidine at the C-terminal (Fig. 1C), and examined its heme-binding ability and heme-degradation activity. The absorption spectrum of the heme-reconstituted G165HG mutant was indistinguishable from that of the heme-G165H mutant (Fig. 6D). Verdoheme was formed following reaction of the heme-G165HG mutant with H_2O_2, but the amount (52% of *Vc*HutZ) was less than that of the K164H mutant (Fig. 6E), suggesting that the enzymatic activity was not improved by the mutation. The absorbance of the Soret band for the heme-G165G and heme-G165HG mutants after the reaction with H_2O_2 (Fig. 6C, D) was smaller than that of the heme-K164H mutant (Fig. 4B). Considering that the amounts of verdoheme in the G165G and G165HG mutants estimated by

the absorbance at 653 nm were less than that of the K164H mutant, heme in these two mutants was randomly broken by OH radical generated by the reaction of heme with H_2O_2. These results imply that histidine at position 164 is the most favorable location for heme binding and verdoheme formation.

3.6. Heme-binding properties and degradation ability of a CTE mutant

To further improve heme-degradation activity, we next focused our attention on the C-terminal sequence of Alr5027. The crystal structure of HugZ from *H. pylori* shows that the C-terminal loop functions as a flexible portion of the active site that serves to keep the substrate heme in a proper conformation for HO activity [21]. Thus, we considered that the C-terminal region of Alr5027 is also important in improving enzymatic activity. A sequence alignment of Alr5027 with HutZ revealed that the sequence of Alr5027 lacks amino acid residues that correspond to the C-terminal region in *Vc*HutZ. Accordingly, we prepared an Alr5027 mutant containing a C-terminal extension (CTE) that mimics the C-terminal region of *Vc*HutZ (Fig. 1A) by inserting the sequence His-Arg-Lys-Ile-Ser between Asp163 and Lys164 (Fig. 1C). Addition of hemin to the CTE mutant yielded a Soret band at 412 nm in the resultant solution that was indistinguishable from that of the heme-K164H mutant (Fig. S5A). A titration curve clearly indicated that the CTE mutant was capable of binding to heme. The calculated $K_{d,heme}$ for the CTE mutant was 0.31 ± 0.07 μM (Fig. S5A, inset), a value comparable to that of the K164H mutant (0.24 ± 0.03 μM).

After the addition of H_2O_2 to the heme-CTE mutant, the absorbance at 652 nm increased (Fig S5B), indicating that verdoheme accumulated in the reaction with H_2O_2. Addition of pyridine to the reaction solution caused the visible band to shift to 659 nm, suggesting that the β- or δ-*meso* position was cleaved (Fig. S6B), a behavior similar to that of the heme-K164H mutant (Fig. S6A). The heme-degradation reaction of the heme-CTE mutant was also examined using ascorbic acid as an electron source. Under these conditions, the Soret band remained after the addition of ascorbic acid at pH 8.0 and pH 6.0 (Fig. S5C, D), indicating

that heme was not degraded in the reaction with ascorbic acid, as observed in the heme-K164H mutant (Fig. 5).

3.7. Reduction and oxyferrous heme formation of heme-Alr5027

To investigate why the heme-K164H mutant was inactive toward ascorbic acid, we took into account the reaction mechanism of *Vc*HutZ. The heme-degradation reaction of *Vc*HutZ is mainly regulated by three key factors: (i) heme reduction [22], (ii) proton transfer from water molecules to reduced oxyferrous heme [46], and (iii) protomer-protomer interaction [47]. We first focused on heme reduction [factor (i)]. The reaction of heme-HutZ with ascorbic acid proceeds at pH 6.0, but not at pH 8.0. This is partially because the reduction rate of heme (k_{red}), the first step in the heme-degradation reaction of *Vc*HutZ (Fig. S1), is ~3-fold faster at pH 6.0 than at pH 8.0 (Table 1) [46]. Thus, we measured the k_{red} of the heme-K164H mutant at pH 6.0 and 8.0. Fig. S7 shows the time course of absorption changes at pH 8.0 after the addition of ascorbic acid to the ferric heme-K164H mutant in the presence of CO to prevent oxidation to ferric heme. Upon reduction, the Soret maximum at 410 nm underwent a red shift to 418 nm, the same position of the Soret band in the CO-bound heme [46]. The time course of the absorption changes at 418 nm was fit to a single exponential, yielding a k_{red} of 2.8 ± 0.2 h^{-1} at pH 8.0 (Table 1). This value was much smaller than that of human HO (0.55 s^{-1}) [48], but larger than that of *Vc*HutZ at pH 8.0 (1.1 ± 0.5 h^{-1}) and similar to that of *Vc*HutZ at pH 6.0 (3.2 ± 0.3 h^{-1}) [46] (Table 1). When measured at pH 6.0, the k_{red} was 4.0 ± 0.6 h^{-1} (Table 1), showing that the k_{red} of Alr5027 at pH 6.0 and 8.0 were almost the same as that of heme-*Vc*HutZ at pH 6.0 [46]. Thus, based on k_{red} values, the reduction rate of heme does not account for the quite small amount of ascorbic acid-assisted heme-degradation by the heme-K164H mutant.

Once ferrous heme is formed, molecular oxygen can bind to form oxyferrous heme. The formation of oxyferrous heme of the K164H mutant was confirmed by absorption spectrum. Ferric heme-K164H mutant (Fig. S8, red line) was reduced by sodium dithionite under

anaerobic conditions (Fig. S8, blue line). After the formation of ferrous heme, a slight amount of air was added to the solution. The Soret band shifted to 418 nm from 432 nm with Q-bands at 539 and 571 nm (Fig. S8, green line). These peak positions were close to those observed for transient oxyferrous heme of *Vc*HutZ [26]. The presence of a small shoulder at 432 nm and a peak at 674 nm suggested the coexistence of ferrous heme and verdoheme, respectively. In contrast to *Vc*HutZ, whose oxyferrous heme is quite unstable to autoxidation owing to the strong electron donation from proximal histidine [22], Alr5027 can form oxyferrous heme.

3.8. Heme-degradation activity through perturbation of the proton transfer pathway

To improve the heme-degradation activity of the K164H mutant, we next considered proton transfer from water molecules to reduced oxyferrous heme [factor (ii)] [46]. Because replacement of Thr27 of *Vc*HutZ with valine substantially suppressed proton transfer to the reduced oxyferrous [Fe(III)-OO^-] species, we hypothesized that water molecules in the active site of *Vc*HutZ, which are potentially fixed by Thr27, act as proton sources (Fig. S1). A sequence alignment of Alr5027 with HutZ revealed that the sequence of Alr5027 lacks four corresponding amino acid residues, including Thr27 (Fig. 1A). Accordingly, we inserted a Glu-Arg-Lys-Thr (ERKT) sequence between Ser20 and Ala21 in the K164H mutant. At pH 6.0, the Soret maximum of the ferric heme of the resulting heme-ERKT mutant was 405 nm (Fig. S9A), which was almost the same as that of the heme-K164H mutant (Fig. 5B). The intensity of the Soret band was very little diminished after the addition of ascorbic acid at pH 6.0, and no clear band was observed in the 500–800 nm region (Fig. S9A). These spectral changes suggest that the heme-ERKT mutant caused no heme-degradation under these conditions, as observed for the heme-K164H mutant (Fig. 5). A similar lack of ascorbic acid-assisted heme degradation was observed at pH 8.0 (Fig. S9B).

3.9. Structural characterization of heme-K164H and heme-ERKT mutants

Finally, we focused on protomer-protomer interaction [factor (iii)]. We have found that

replacement of Ala31 of *Vc*HutZ with valine at the subunit-subunit interface results in the loss of the ascorbic acid-assisted heme-degradation activity [47]. The elongation of the distance between protomers lead to a decrease in electron donation from the heme axial ligand His170 of *Vc*HutZ that forms a hydrogen bond with nearby Asp132 [47]. Unlike most peroxidases, the hydrogen bond partner (Asp132) of His170 comes from another protomer. Thus, a slight change of relative orientation of protomers modulates the strength of the hydrogen bond between His170 and Asp132, leading to a reduction in electron donation from the proximal histidine to heme. Accordingly, we considered the possibility that the heme in K164H and ERKT mutants was not degraded by ascorbic acid because the distance between the subunits was elongated compared with that in *Vc*HutZ. The distance between subunits can be inferred from the distance between heme and Trp103 (Fig. S10). To estimate the distance between heme and Trp103 of the heme-K164H mutant, we measured the fluorescence spectra of tryptophan. Following excitation at 295 nm, the fluorescence of Trp103, which is the sole tryptophan in Alr5027, was observed at ~334 nm. The fluorescence for the heme-bound K164H mutant was much smaller than that of the heme-unbound K164H mutant (Fig. 7A), suggesting that the fluorescence of Trp103 was quenched by heme. Using the intensity of the fluorescence at 334 nm for the heme-unbound K164H and heme-K164H mutant, we calculated the energy transfer efficiency, E, and estimated the distance between heme and Trp103 on the basis of Equations 2 and 3, respectively. For the K164H mutant, the distance at pH 6.0 was estimated to be 18–22 Å, which is larger than that of heme-WT *Vc*HutZ (16–18 Å) [47]. The fluorescence of the ERKT mutant was also significantly decreased upon heme binding, and the estimated distance of 17–22 Å (Fig. 7B, C) was larger than that of heme-WT *Vc*HutZ [47]. These results suggest that the diminished heme-degradation activity of the ERKT mutant when ascorbic acid is used as an electron source is also related to elongation of the distance between heme and Trp103, as observed in the heme-K164H mutant Alr5027 and heme-A31V mutant *Vc*HutZ [47].

3.10. Heme-degradation activity following introduction of alanine at the subunit-subunit interface

Because a sequence alignment revealed that Ser24 of Alr5027 corresponds to Ala31 in *Vc*HutZ (Fig. 1A), we predicted that replacement of Ser24 with alanine in the ERKT mutant would reduce the distance between protomers at pH 6.0 and lead to enhanced heme degradation by ascorbic acid. Accordingly, we replaced Ser24 with alanine in the ERKT mutant and measured the fluorescence spectra of tryptophan (Fig. 7D). We also calculated the energy transfer efficiency, *E*, and the distance, using the fluorescence intensity at 334 nm of heme-bound and unbound S24A/ERKT mutant. The estimated distance was 17–23 Å (Fig. 7B, D), which is similar to that of the ERKT mutant. The heme-degradation reaction of the S24A/ERKT mutant was also examined using ascorbic acid. The Soret band remained even after the addition of ascorbic acid at both pH 6.0 and pH 8.0 (Fig. S11), indicating that heme was not degraded in the reaction with ascorbic acid. This is because the distance between protomers at pH 6 was still greater than optimal.

3.11. Biliverdin formation by the K164H mutant

Once verdoheme is produced in HOs and *Vc*HutZ, further oxidation leads to the production of biliverdin [22]. To confirm the formation of biliverdin from verdoheme, we treated the verdoheme of the K164H mutant, which was formed by the reaction with H_2O_2, with ascorbic acid. The maximum of the visible band shifted from 652 to 672 nm within 5 min (Fig. 8A), indicating the conversion of ferric verdoheme to ferrous verdoheme, as observed in *Vc*HutZ [26]. Thereafter, the intensity of the 672-nm band gradually decreased. Addition of ferrozine, which forms a stable complex with ferrous iron, to the product caused the appearance of a new band at 562 nm, typical of the Fe^{2+}-ferrozine complex, indicating that ferrous iron was released (Fig. 8A). Although biliverdin was not formed and Fe^{2+} was not released by the reaction of the K164H mutant with only ascorbic acid, simultaneous treatment with H_2O_2 and ascorbic acid yielded biliverdin and free Fe^{2+}, indicating that Alr5027 obtained ability to

degrade heme to produce biliverdin by mutating Lys164 with histidine.

The regioselectivity of the heme breakage was determined by high-performance liquid chromatography (HPLC) analysis of the products. Biliverdin IXα, IXβ, IXδ and IXγ isomers, produced from the reaction of free heme with ascorbic acid, corresponded to peaks at 15.5, 21.1, 23.3, and 32.7 min, respectively, in the HPLC chromatogram (Fig. 8B). Peaks were assigned on the basis of a previous report [37]. In the chromatogram of the K164H mutant, two large peaks appeared at 21.3 and 23.4 min, which corresponded to biliverdin IXβ and biliverdin IXδ, respectively (Fig. 8B). Thus, the cleavage site of biliverdin produced by the K164H mutant was the β- or δ-*meso* position, which is the same as that of *Vc*HutZ [22].

4. Conclusion

We previously found that HutZ from *V. cholerae* has heme-degrading ability and produces the same reaction products as HOs [22,26,31]. The structure of heme-bound HugZ from *H. pylori* suggests that members of the HugZ family are structurally distinct from HOs (Fig. S2). Thus, we predicted that the ancestor protein of HutZ is different from that of canonical HOs. In the current study, we found that Alr5027 from *Nostoc* sp. PCC 7120 is homologous to HutZ (Fig. 1A) and belongs in a phylogenetic group apart from other HutZ family members (Fig. 1B). Characterization of the heme-binding ability and heme-degradation activity of Alr5027 showed that Alr5027 did not bind to heme (Fig. 3), because the heme axial histidine ligand was not conserved in Alr5027 (Fig. 1A). However, introduction of histidine at position at 164 conferred heme-binding ability on Alr5027. Although none of the mutants degraded heme with ascorbic acid because of elongation of the distance between the subunits (Fig. 7), the K164H and G165H mutants formed verdoheme with H_2O_2. Furthermore, by the addition of ascorbic acid to verdoheme in the K164H mutant, β- or δ-biliverdin was produced and Fe^{2+} was released (Fig. 8). Some heme proteins such as myoglobin and cytochrome b_5 also form biliverdin through the reaction with ascorbic acid in the absence of catalase known as coupled

oxidation [49–51]. In this reaction, H_2O_2 produced by ascorbic acid attacks oxy-myoglobin to form biliverdin [52]. Verdoheme is not formed but instead high-valent Fe^{IV}=O species are formed [40,41]. Therefore, the reaction mechanism of coupled oxidation is different from that of HOs in spite of the same final products. Verdoheme formation without high-valent species is a characteristic feature of heme-degrading enzymes. Our results indicate that a lysine-to-histidine substitution at residue 164 was the mutation that most effectively enabled Alr5027 to bind heme and produce verdoheme and biliverdin conditionally (Fig. 4). Although we cannot rule out the possibility that the ancestor protein of Alr5027 has lost the heme-degradation ability, our findings suggest that pathogenic bacteria that possess HutZ family members may have acquired heme-degradation ability from a common ancestor of Alr5027 through molecular evolution.

Abbreviations

*Vc*HutZ	HutZ from *Vibrio cholerae*
HO	heme oxygenase
CO	carbon monoxide
WT	wild-type

Acknowledgements

The authors thank Y. Nakamura (Hokkaido University) for helping to measure absorption spectrum of oxyferrous heme for K164H mutant Alr5027. This study was supported in part by Grants-in-Aid for Scientific Research (18J10820 to N.D., 16K05835 to T.U., and 19H05769 to K.I.) from the Ministry of Culture, Education, Sports, Science, and Technology (MEXT) of Japan.

Appendix A. Supplementary data

Supplementary data to this article can be found online at

References

[1] R. Tenhunen, H.S. Marver, R. Schmid, Microsomal heme oxygenase. Characterization

of the enzyme., J. Biol. Chem. 244 (1969) 6388–6394.

[2] T. Yoshida, G. Kikuchi, Features of the reaction of heme degradation catalyzed by the reconstituted microsomal heme oxygenase system., J. Biol. Chem. 253 (1978) 4230–4236.

[3] P.R. Ortiz de Montellano, Heme oxygenase mechanism: Evidence for an electrophilic, ferric peroxide species, Acc. Chem. Res. 31 (1998) 543–549. doi:10.1021/ar960207q.

[4] A. Ayer, A. Zarjou, A. Agarwal, R. Stocker, Heme oxygenases in cardiovascular health and disease., Physiol. Rev. 96 (2016) 1449–1508. doi:10.1152/physrev.00003.2016.

[5] R. Gozzelino, V. Jeney, M.P. Soares, Mechanisms of cell protection by heme oxygenase-1., Annu. Rev. Pharmacol. Toxicol. 50 (2010) 323–354. doi:10.1146/annurev.pharmtox.010909.105600.

[6] S.J. Davis, J. Kurepa, R.D. Vierstra, The Arabidopsis thaliana HY1 locus, required for phytochrome-chromophore biosynthesis, encodes a protein related to heme oxygenases, Proc. Natl. Acad. Sci. 96 (1999) 6541–6546. doi:10.1073/pnas.96.11.6541.

[7] H. Contreras, N. Chim, A. Credali, C.W. Goulding, Heme uptake in bacterial pathogens, Curr. Opin. Chem. Biol. 19 (2014) 34–41. doi:10.1016/j.cbpa.2013.12.014.

[8] G. Pishchany, E.P. Skaar, Taste for blood: Hemoglobin as a nutrient source for pathogens, PLoS Pathog. 8 (2012) 1–4. doi:10.1371/journal.ppat.1002535.

[9] N.D. Hammer, E.P. Skaar, Molecular mechanisms of Staphylococcus aureus iron acquisition., Annu. Rev. Microbiol. 65 (2011) 129–147. doi:10.1146/annurev-micro-090110-102851.

[10] E.P. Skaar, M. Humayun, T. Bae, K.L. DeBord, O. Schneewind, Iron-source preference of Staphylococcus aureus infections., Science. 305 (2004) 1626–1628. doi:10.1126/science.1099930.

[11] A. Wilks, K.A. Burkhard, Heme and virulence: how bacterial pathogens regulate,

transport and utilize heme, Nat. Prod. Rep. 24 (2007) 511–522. doi:10.1039/b604193k.

[12] S. Hirotsu, G.C. Chu, M. Unno, D.-S. Lee, T. Yoshida, S.-Y. Park, Y. Shiro, M. Ikeda-Saito, The crystal structures of the ferric and ferrous forms of the heme complex of HmuO, a heme oxygenase of Corynebacterium diphtheriae., J. Biol. Chem. 279 (2004) 11937–11947. doi:10.1074/jbc.M311631200.

[13] D.J. Schuller, W.M. Zhu, I. Stojiljkovic, A. Wilks, T.L. Poulos, Crystal structure of heme oxygenase from the Gram-negative pathogen Neisseria meningitidis and a comparison with mammalian heme oxygenase-1, Biochemistry. 40 (2001) 11552–11558. doi:10.1021/bi0110239.

[14] J. Friedman, L. Lad, H. Li, A. Wilks, T.L. Poulos, Structural basis for novel δ-regioselective heme oxygenation in the opportunistic pathogen Pseudomonas aeruginosa, Biochemistry. 43 (2004) 5239–5245. doi:10.1021/bi049687g.

[15] D.J. Schuller, A. Wilks, P.R. Ortiz de Montellano, T.L. Poulos, Crystal structure of human heme oxygenase-1., Nat. Struct. Biol. 6 (1999) 860–867. doi:10.1038/12319.

[16] T. Matsui, M. Unno, M. Ikeda-Saito, Heme oxygenase reveals its strategy for catalyzing three successive oxygenation reactions, Acc. Chem. Res. 43 (2010) 240–247. doi:10.1021/ar9001685.

[17] R. Wu, E.P. Skaar, R. Zhang, G. Joachimiak, P. Gornicki, O. Schneewind, A. Joachimiak, Staphylococcus aureus IsdG and IsdI, heme-degrading enzymes with structural similarity to monooxygenases, J. Biol. Chem. 280 (2005) 2840–2846. doi:10.1074/jbc.M409526200.

[18] T. Matsui, S. Nambu, C.W. Goulding, S. Takahashi, H. Fujii, M. Ikeda-Saito, Unique coupling of mono- and dioxygenase chemistries in a single active site promotes heme degradation, Proc. Natl. Acad. Sci. U. S. A. 113 (2016) 3779–3784. doi:10.1073/pnas.1523333113.

[19] T. Matsui, S. Nambu, Y. Ono, C.W. Goulding, K. Tsumoto, M. Ikeda-Saito, Heme degradation by Staphylococcus aureus IsdG and IsdI liberates formaldehyde rather than carbon monoxide, Biochemistry. 52 (2013) 3025–3027. doi:10.1021/bi400382p.

[20] R. Zhang, J. Zhang, G. Guo, X. Mao, W. Tong, Y. Zhang, D.C. Wang, Y. Hu, Q. Zou, Crystal structure of Campylobacter jejuni ChuZ: A split-barrel family heme oxygenase with a novel heme-binding mode, Biochem. Biophys. Res. Commun. 415 (2011) 82–87. doi:10.1016/j.bbrc.2011.10.016.

[21] Y. Hu, F. Jiang, Y. Guo, X. Shen, Y. Zhang, R. Zhang, G. Guo, X. Mao, Q. Zou, D.-C. Wang, Crystal structure of HugZ, a novel heme oxygenase from Helicobacter pylori., J. Biol. Chem. 286 (2011) 1537–1544. doi:10.1074/jbc.M110.172007.

[22] T. Uchida, Y. Sekine, T. Matsui, M. Ikeda-Saito, K. Ishimori, A heme degradation enzyme, HutZ, from Vibrio cholerae, Chem. Commun. 48 (2012) 6741–6743. doi:10.1039/c2cc31147j.

[23] E.E. Wyckoff, M. Schmitt, A. Wilks, S.M. Payne, HutZ is required for efficient heme utilization in Vibrio cholerae, J. Bacteriol. 186 (2004) 4142–4151. doi:10.1128/JB.186.13.4142.

[24] M. Unno, T. Matsui, M. Ikeda-Saito, Structure and catalytic mechanism of heme oxygenase, Nat. Prod. Rep. 24 (2007) 553–570. doi:10.1039/b604180a.

[25] G. Kikuchi, T. Yoshida, M. Noguchi, Heme oxygenase and heme degradation, Biochem. Biophys. Res. Commun. 338 (2005) 558–567. doi:10.1016/j.bbrc.2005.08.020.

[26] T. Uchida, Y. Sekine, N. Dojun, A. Lewis-Ballester, I. Ishigami, T. Matsui, S.-R. Yeh, K. Ishimori, Reaction intermediates in the heme degradation reaction by HutZ from Vibrio cholerae, Dalt. Trans. 46 (2017) 8104–8109. doi:10.1039/C7DT01562C.

[27] B. Rasmussen, I.R. Fletcher, J.J. Brocks, M.R. Kilburn, Reassessing the first

appearance of eukaryotes and cyanobacteria, Nature. 455 (2008) 1101–1104. doi:10.1038/nature07381.

[28] J. Raymond, R.R.E. Blankenship, Biosynthetic pathways, gene replacement and the antiquity of life, Geobiology. 2 (2004) 199–203. doi:10.1111/j.1472-4677.2004.00037.x.

[29] T. Domitrovic, D.P. Raymundo, T.F. da Silva, F.L. Palhano, Experimental evidence for a revision in the annotation of putative pyridoxamine 5'-phosphate oxidases P(N/M)P from Fungi., PLoS One. 10 (2015) e0136761. doi:10.1371/journal.pone.0136761.

[30] T. Kaneko, Y. Nakamura, C.P. Wolk, T. Kuritz, S. Sasamoto, A. Watanabe, M. Iriguchi, A. Ishikawa, K. Kawashima, T. Kimura, Y. Kishida, M. Kohara, M. Matsumoto, A. Matsuno, A. Muraki, N. Nakazaki, S. Shimpo, M. Sugimoto, M. Takazawa, M. Yamada, M. Yasuda, S. Tabata, Complete genomic sequence of the filamentous nitrogen-fixing cyanobacterium Anabaena sp. strain PCC 7120, DNA Res. 8 (2001) 205–253.

[31] T. Uchida, N. Dojun, Y. Sekine, K. Ishimori, Heme proximal hydrogen bonding between His170 and Asp132 plays an essential role in the heme degradation reaction of HutZ from Vibrio cholerae, Biochemistry. 56 (2017) 2723–2734. doi:10.1021/acs.biochem.7b00152.

[32] S. Kumar, G. Stecher, K. Tamura, MEGA7: Molecular Evolutionary Genetics Analysis Version 7.0 for Bigger Datasets., Mol. Biol. Evol. 33 (2016) 1870–1874. doi:10.1093/molbev/msw054.

[33] T. Uchida, M. Sasaki, Y. Tanaka, K. Ishimori, A dye-decolorizing peroxidase from Vibrio cholerae, Biochemistry. 54 (2015) 6610–6621. doi:10.1021/acs.biochem.5b00952.

[34] E.A. Berry, B.L. Trumpower, Simultaneous determination of hemes *a*, *b*, and *c* from

pyridine hemochrome spectra., Anal. Biochem. 161 (1987) 1–15. doi:10.1016/0003-2697(87)90643-9.

[35] P. Wu, L. Brand, Resonance energy transfer: methods and applications., Anal. Biochem. 218 (1994) 1–13. http://www.ncbi.nlm.nih.gov/pubmed/8053542 (accessed October 11, 2017).

[36] X. Zhang, H. Fujii, K.M. Matera, C.T. Migita, D. Sun, M. Sato, M. Ikeda-Saito, T. Yoshida, Stereoselectivity of each of the three steps of the heme oxygenase reaction: hemin to meso-hydroxyhemin, meso-hydroxyhemin to verdoheme, and verdoheme to biliverdin., Biochemistry. 42 (2003) 7418–7426. doi:10.1021/bi027173g.

[37] H. Sakamoto, Y. Omata, Y. Adachi, G. Palmer, M. Noguchi, Separation and identification of the regioisomers of verdoheme by reversed-phase ion-pair high-performance liquid chromatography, and characterization of their complexes with heme oxygenase, J. Inorg. Biochem. 82 (2000) 113–121. doi:10.1016/S0162-0134(00)00149-5.

[38] S.W. Englander, D.B. Calhoun, J.J. Englander, Biochemistry without oxygen., Anal. Biochem. 161 (1987) 300–306. doi:10.1016/0003-2697(87)90454-4.

[39] M. Sugishima, H. Sato, Y. Higashimoto, J. Harada, K. Wada, K. Fukuyama, M. Noguchi, Structural basis for the electron transfer from an open form of NADPH-cytochrome P450 oxidoreductase to heme oxygenase, Proc. Natl. Acad. Sci. U. S. A. 111 (2014) 2524–2529. doi:10.1073/pnas.1322034111.

[40] N.K. King, M.E. Wingield, The mechanism of metmyoglobin oxidation., J. Biol. Chem. 238 (1963) 1520–8.

[41] A. Wilks, P.R. Ortiz de Montellano, Intramolecular translocation of the protein radical formed in the reaction of recombinant sperm whale myoglobin with H2O2., J. Biol. Chem. 267 (1992) 8827–8833. doi:10.1016/j.japwor.2012.04.003.

[42] T. Yonetani, H. Schleyer, Studies on cytochrome c peroxidase: IX. The reaction of ferrimyoglobin with hydroperoxides and a comparison of peroxide-induced compounds of ferrimyoglobin and cytochrome c peroxidase, J. Biol. Chem. 242 (1967) 1974–1979.

[43] N. Kelso King, F.D. Looney, M.E. Winfield, Amino acid free radicals in oxidised metmyoglobin, BBA - Protein Struct. 133 (1967) 65–82. doi:10.1016/0005-2795(67)90039-6.

[44] T. Egawa, H. Shimada, Y. Ishimura, Formation of compound I in the reaction of native myoglobins with hydrogen peroxide, J. Biol. Chem. 275 (2000) 34858–34866. doi:10.1074/jbc.M004026200.

[45] Y. Liu, L. Koenigs Lightning, H. Huang, P. Moënne-Loccoz, D.J. Schuller, T.L. Poulos, T.M. Loehr, P.R. Ortiz de Montellano, Replacement of the distal glycine 139 transforms human heme oxygenase-1 into a peroxidase., J. Biol. Chem. 275 (2000) 34501–34507. doi:10.1074/jbc.M004245200.

[46] N. Dojun, Y. Sekine, K. Ishimori, T. Uchida, Iron chelators inhibit the heme-degradation reaction by HutZ from Vibrio cholerae, Dalt. Trans. 46 (2017) 5147–5150. doi:10.1039/C7DT00121E.

[47] T. Uchida, K. Ota, Y. Sekine, N. Dojun, K. Ishimori, Subunit-subunit interactions play a key role in the heme-degradation reaction of HutZ from Vibrio cholerae, Dalt. Trans. 48 (2019) 3973–3983. doi:10.1039/C9DT00604D.

[48] Y. Liu, P.R. Ortiz de Montellano, Reaction intermediates and single turnover rate constants for the oxidation of heme by human heme oxygenase-1, J. Biol. Chem. 275 (2000) 5297–5307. doi:10.1074/jbc.275.8.5297.

[49] S.B. Brown, Stereospecific haem cleavage. A model for the formation of bile pigment isomers in vivo and in vitro, Biochem. J. 159 (1976) 23–27. doi:10.1042/bj1590023.

[50] P.O. 'Carra, E. Colleran, HAEM catabolism and coupled oxidation of haemproteins,

FEBS Lett. 5 (1969) 295–298.

[51] J.C. Rodríguez, M. Rivera, Conversion of mitochondrial cytochrome b5 into A species capable of performing the efficient coupled oxidation of heme, Biochemistry. 37 (1998) 13082–13090. doi:10.1021/bi9809324.

[52] J.A. Sigman, X. Wang, Y. Lu, Coupled oxidation of heme by myoglobin is mediated by exogenous peroxide, J. Am. Chem. Soc. 123 (2001) 6945–6946.

Table

Table 1

Heme reduction rate constant (k_{red}) of ferric heme iron for Alr5027 mutant and HutZ

Proteins		k_{red} (h^{-1})		Ref.
		pH 8.0	pH 6.0	
Alr5027	K164H	2.8 ± 0.2	4.0 ± 0.6	this study
HutZ	WT	1.1 ± 0.5	3.2 ± 0.3	[46]
Human HO	WT	2.0×10^3 [a]		[48]

[a] Measured at pH 7.9.

Figure legends

Fig 1. Sequence alignment of Alr5027. (A) Sequence alignment of the HutZ family and Alr5027. The alignment was performed using ClustalW2 (http://www.ebi.ac.uk/Tools/msa/clustalw2/). The active site arginine, aspartate, and histidine are shown in red bold type. Proteins used in the alignment are (from top to bottom) *Aeromonas hydrophila* subsp. *hydrophila* ATCC 7966 HutZ, *Plesiomonas shigelloides* HugZ, *Histophilus somni* HutZ, *multocida* str. Pm70 PM0299, *Mannheimia haemolytica* PHL213 HugZ, *Vibrio cholerae* HutZ, and *Nostoc* sp. PCC 7120 Alr5027. (B) Phylogenetic tree of Alr5027 with the HutZ family. The tree was obtained from the sequence alignment in Fig 1A. The maximum likelihood method was used for tree construction and bootstrap analysis (parameter set at 1000 resampling), performed using MEGA 7 software. (C) Alignment of WT and mutant Alr5027 in the C-terminal region (163–165).

Fig 2. Purification of Alr5027. (A) SDS-PAGE gel of purified Alr5027 stained with Coomassie Brilliant Blue, including molecular mass marker (lane M), whole-cell protein extracts (lane 1), purified His-tagged Alr5027 (lane 2), purified His-tag–cleaved Alr5027 (lane 3), and purified Alr5027 after gel-filtration chromatography (lane 4). (B) Profile of Alr5027 on a gel-filtration column pre-equilibrated with 50 mM Tris-HCl and 150 mM NaCl (pH 8.0). The retention volumes of standard proteins were as follows: thyroglobulin, 50.0 mL; ferritin, 56.4 mL; catalase, 66.7 mL; aldose, 67.5 mL; albumin, 76.3 mL; ovalbumin, 81.8 mL; chymotrypsinogen A, 92.5 mL; and RNase A, 97.6 mL.

Fig 3. Absorption spectra of the heme-WT Alr5027 complex. Spectra are for purified apo-Alr5027 (red line), free heme (black line), and heme-Alr5027 (blue line). The inset shows differences at 414 nm following incremental addition of heme (2–30 μM) to Alr5027 (10 μM) in 50 mM Tris-HCl and 150 mM NaCl (pH 8.0), measured against a blank cell containing buffer alone.

Fig 4. Absorption spectra and chromatogram of the heme-K164H mutant. (A) Absorption spectra of the heme-K164H mutant (red line) and WT Alr5027 (black line) at pH 8.0. The inset shows differences at 414 nm following incremental addition of heme (2–30 mM) to the mutant (10 mM) in 50 mM Tris-HCl and 150 mM NaCl (pH 8.0), measured against a blank cell containing buffer alone. (B, C) Heme-degradation reaction of the heme-K164H mutant (B) and heme-WT Alr5027 (C) reacted with 0.1 mM H_2O_2 at pH 8.0. Spectra were obtained before and after the addition of H_2O at 1-min intervals over 10 min.

Fig 5. Heme-degradation reaction of the K164H mutant with ascorbic acid. (A) pH 8.0 and (B) pH 6.0. Spectra were recorded before the addition of ascorbic acid, and at 2-min intervals for 30 min after the addition of ascorbic acid. The concentrations of the protein and ascorbic acid were 5 μM and 1.0 mM, respectively.

Fig 6. Absorption spectra of the D163H, G165H, and G165HG mutants. (A, B) Absorption spectra of heme-D163H (A) and heme-G165H (B) mutants at pH 8.0. The inset shows differences at 414 nm following incremental addition of heme (2–30 μM) to Alr5027 (10 μM) in 50 mM Tris-HCl and 150 mM NaCl (pH 8.0), measured against a blank cell containing buffer alone. (C) Heme-degradation reaction of the heme-G165H mutant with H_2O_2 (0.1 mM) at pH 8.0. Spectra were measured before and after the addition of H_2O_2 at 1-min intervals for 10 min. (D) Absorption spectrum of the heme-G165HG mutant at pH 8.0. (E) Heme-degradation reaction of the G165HG mutant with H_2O_2. The reaction conditions were same as those in (C).

Fig 7. Fluorescence spectra of heme-K164H (A), heme-ERKT (C) and heme-S24A/ERKT Alr5027 mutants (D) in the absence (blue lines) and presence (red lines) of heme. Spectra were recorded at pH 6.0, 6.2, 6.3, 6.4, 6.6, 6.8, 7.0, 7.5, 8.0, 8.5 and 8.8, with excitation at 295 nm. The sample concentration was 5 μM. (B) pH dependence of the distance between heme and Trp103 in K164H, ERKT, and S24A/ERKT mutants.

Fig 8. Heme degradation of the K164H mutant using H_2O_2 and ascorbic acid. (A) Reaction of the verdoheme-K164H mutant with 1 mM ascorbic acid at pH 8.0. Absorption spectra in the reaction with ascorbic acid after the formation of verdoheme (blue line) by addition of 0.1 mM H_2O_2. Spectra were recorded before and after the addition of ascorbic acid at 4, 8, 16, 24, and 32 min (black line). Ferrozine (0.10 mM) was added 32 min after the reaction (green line). (B) HPLC chromatograms of biliverdin standard (red line) and final products of the heme-K164H mutant (blue line) monitored at 380 nm.

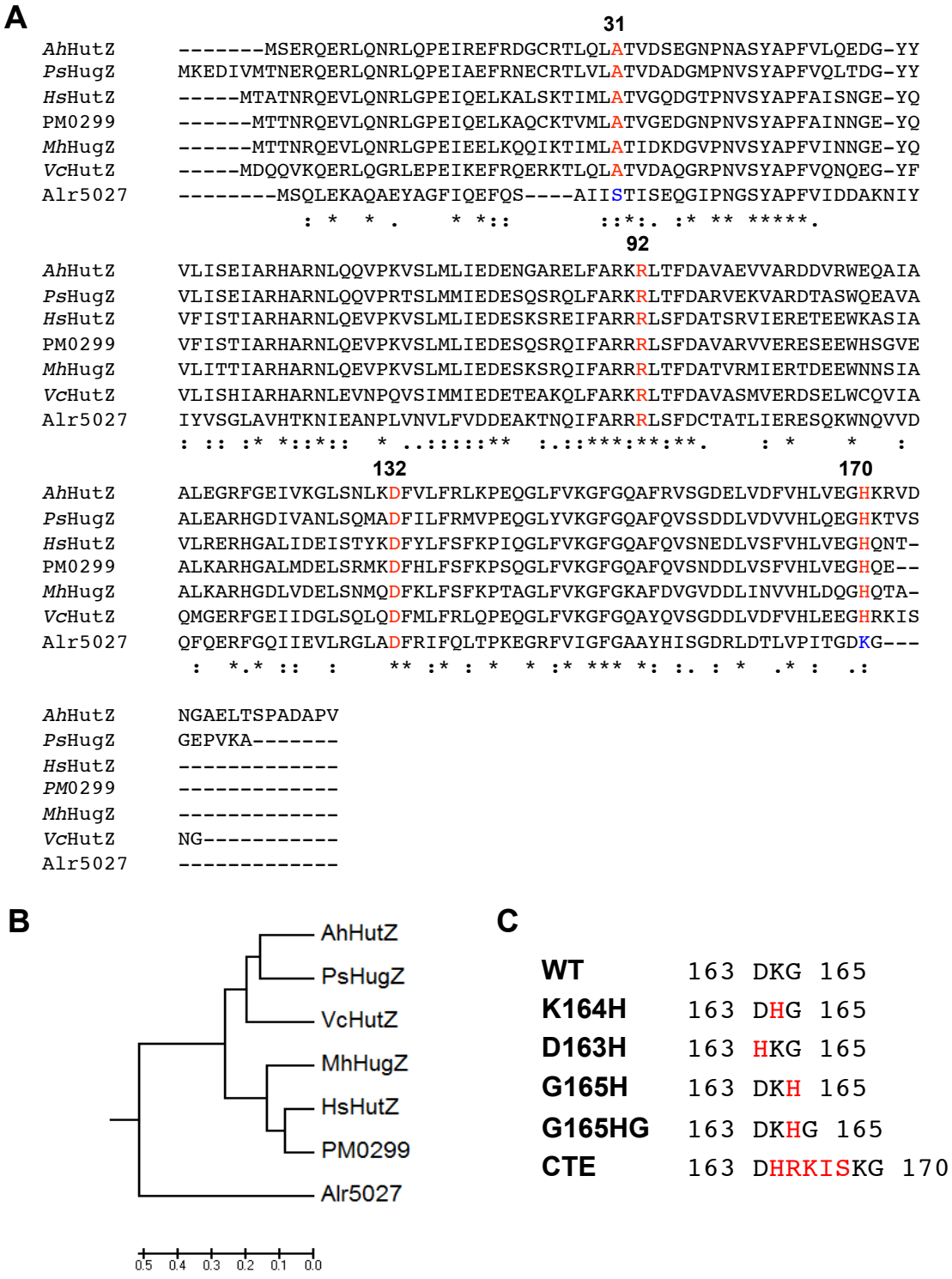

Fig. 1. Sequence alignment of Alr5027. (A) Sequence alignment of the HutZ family and Alr5027. The alignment was performed using ClustalW2 (http://www.ebi.ac.uk/Tools/msa/clustalw2/). The active site arginine, aspartate, and histidine are shown in red bold type. Proteins used in the alignment are (from top to bottom) *Aeromonas hydrophila* subsp. *hydrophila* ATCC 7966 HutZ, *Plesiomonas shigelloides* HugZ, *Histophilus somni* HutZ, *multocida* str. Pm70 PM0299, *Mannheimia haemolytica* PHL213 HugZ, *Vibrio cholerae* HutZ, and *Nostoc* sp. PCC 7120 Alr5027. (B) Phylogenetic tree of Alr5027 with the HutZ family. The tree was obtained from the sequence alignment in Fig 1A. The maximum likelihood method was used for tree construction and bootstrap analysis (parameter set at 1000 resampling), performed using MEGA 7 software. (C) Alignment of Alr5027 WT and mutants in the C-terminal region (163–165).

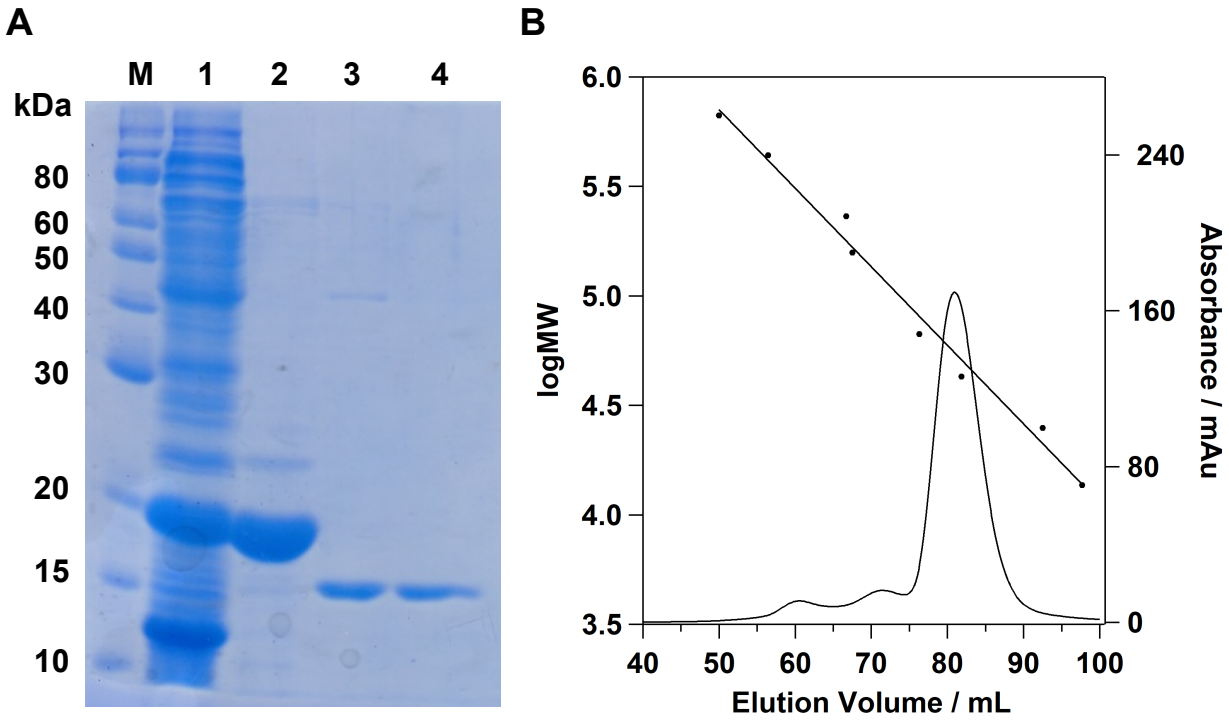

Fig. 2. Purification of Alr5027. (A) SDS-PAGE gel of purified Alr5027 stained with Coomassie Brilliant Blue, including molecular mass marker (lane M), whole-cell protein extracts (lane 1), purified His-tagged Alr5027 (lane 2), purified His-tag–cleaved Alr5027 (lane 3), and purified Alr5027 after gel-filtration chromatography (lane 4). (B) Profile of Alr5027 on a gel-filtration column pre-equilibrated with 50 mM Tris-HCl and 150 mM NaCl (pH 8.0). The retention volumes of standard proteins were as follows: thyroglobulin, 50.0 mL; ferritin, 56.4 mL; catalase, 66.7 mL; aldose, 67.5 mL; albumin, 76.3 mL; ovalbumin, 81.8 mL; chymotrypsinogen A, 92.5 mL; and RNase A, 97.6 mL.

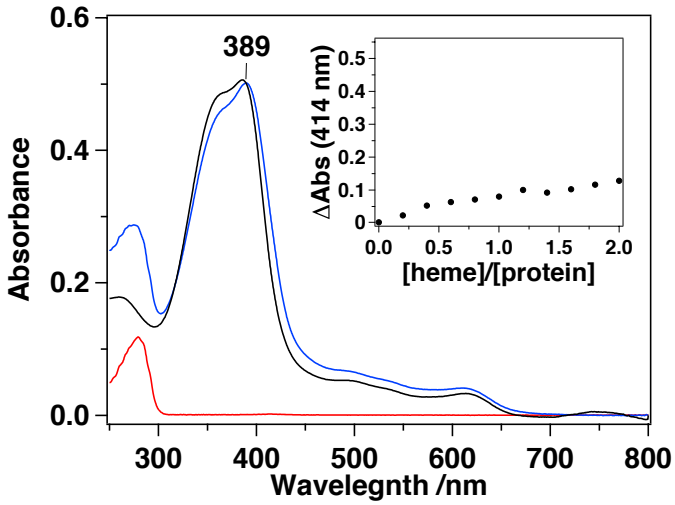

Fig. 3. Absorption spectra of the heme-WT Alr5027 complex. Spectra are for purified apo-Alr5027 (red line), free heme (black line), and heme-Alr5027 (blue line). The inset shows differences at 414 nm following incremental addition of heme (2–30 μM) to Alr5027 (10 μM) in 50 mM Tris-HCl and 150 mM NaCl (pH 8.0), measured against a blank cell containing buffer alone.

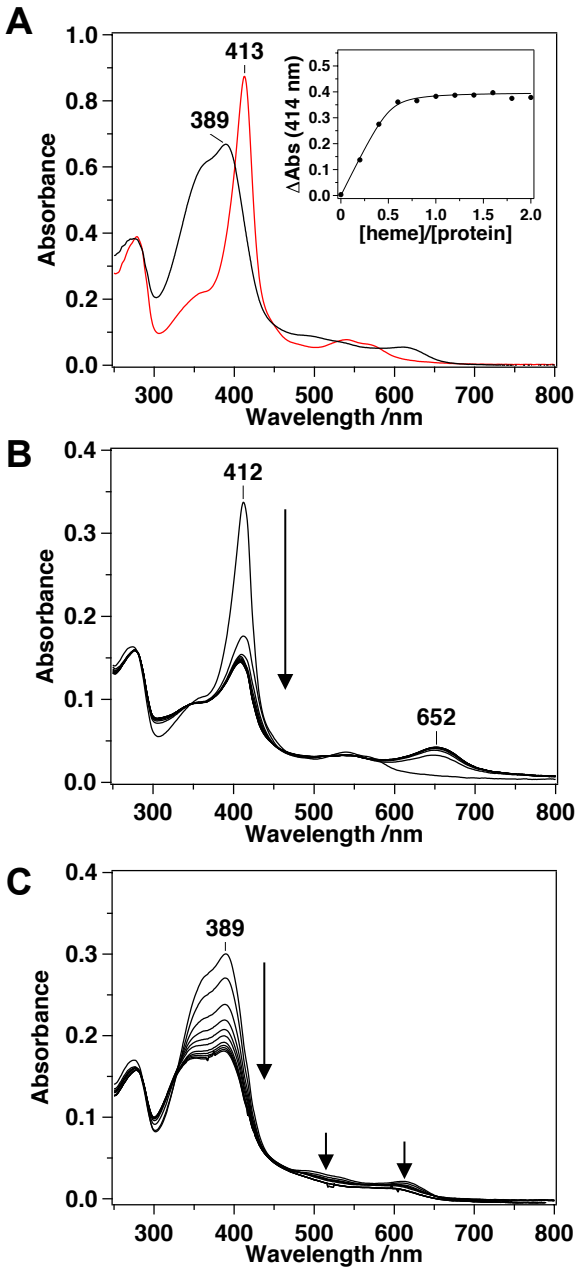

Fig. 4. Absorption spectra and chromatogram of the heme-K164H mutant. (A) Absorption spectra of the heme-K164H mutant (red line) and WT alr5027 (black line) at pH 8.0. The inset shows differences at 414 nm following incremental addition of heme (2–30 μM) to the mutant (10 μM) in 50 mM Tris-HCl and 150 mM NaCl (pH 8.0), measured against a blank cell containing buffer alone. (B, C) Heme-degradation reaction of the heme-K164H mutant (B) and heme-WT Alr5027 (C) reacted with 0.1 mM H_2O_2 at pH 8.0. Spectra were obtained before and after the addition of H_2O at 1-min intervals over 10 min.

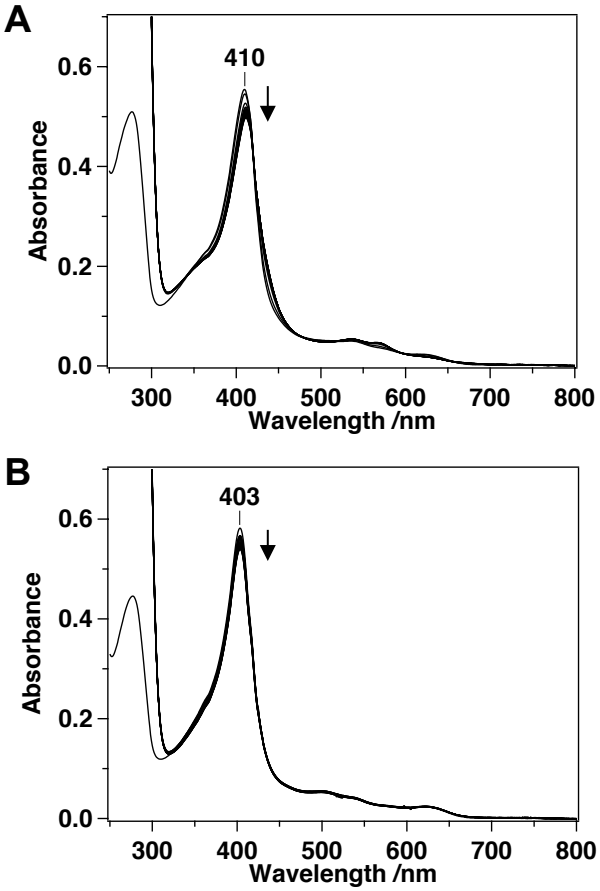

Fig 5. Heme-degradation reaction of the K164H mutant with ascorbic acid. (A) pH 8.0 and (B) pH 6.0. Spectra were recorded before the addition of ascorbic acid, and at 2-min intervals for 30 min after the addition of ascorbic acid. The concentrations of the protein and ascorbic acid were 5 μM and 1.0 mM, respectively.

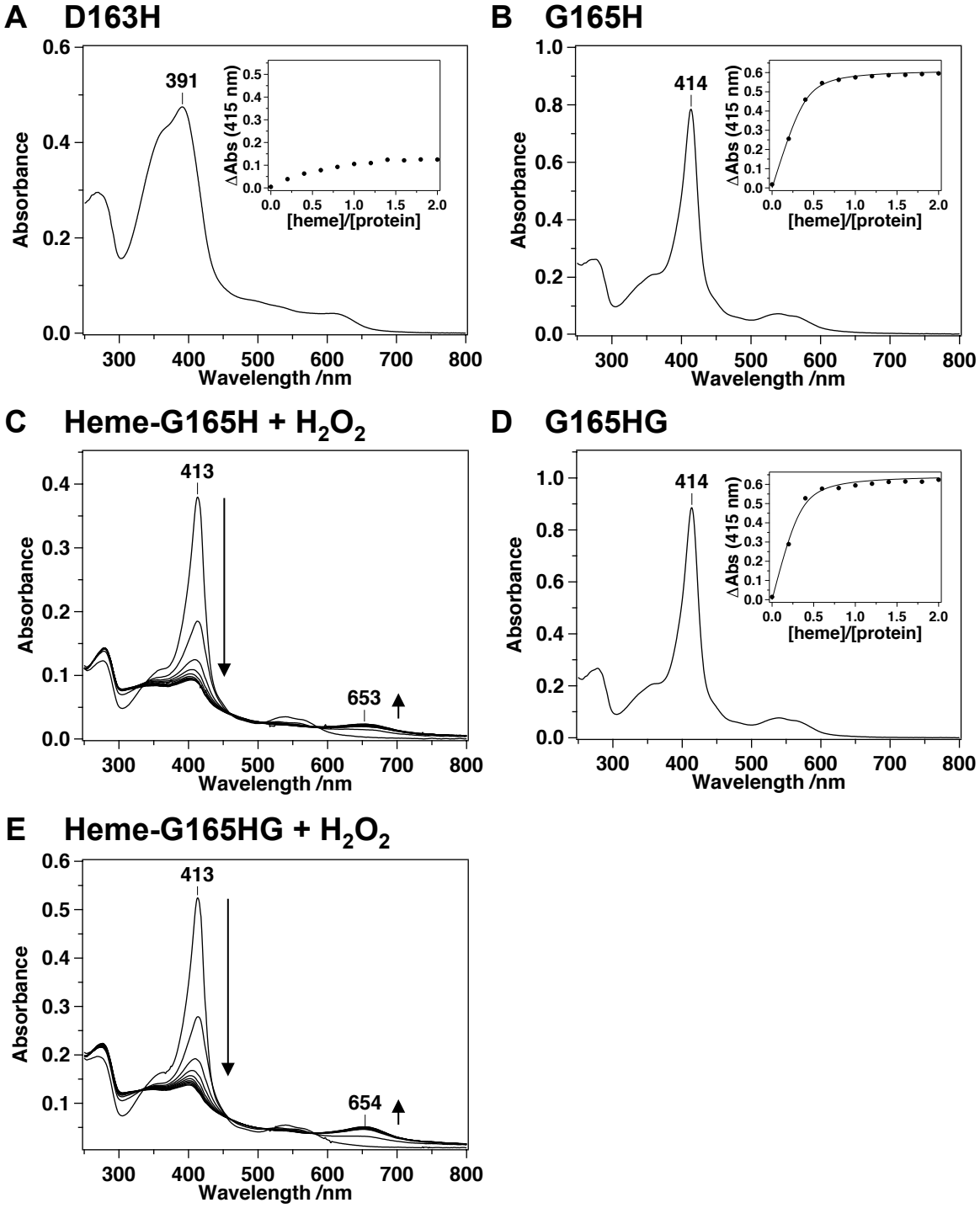

Fig. 6. Absorption spectra of the D163H, G165H, and G165HG mutants. (A, B) Absorption spectra of heme-D163H (A) and heme-G165H (B) mutants at pH 8.0. The inset shows differences at 414 nm following incremental addition of heme (2–30 μM) to Alr5027 (10 μM) in 50 mM Tris-HCl and 150 mM NaCl (pH 8.0), measured against a blank cell containing buffer alone. (C) Heme-degradation reaction of the heme-G165H mutant with H_2O_2 (0.1 mM) at pH 8.0. Spectra were measured before and after the addition of H_2O_2 at 1-min intervals for 10 min. (D) Absorption spectrum of the heme-G165HG mutant at pH 8.0. (E) Heme-degradation reaction of the G165HG mutant with H_2O_2. The reaction conditions were same as those in (C).

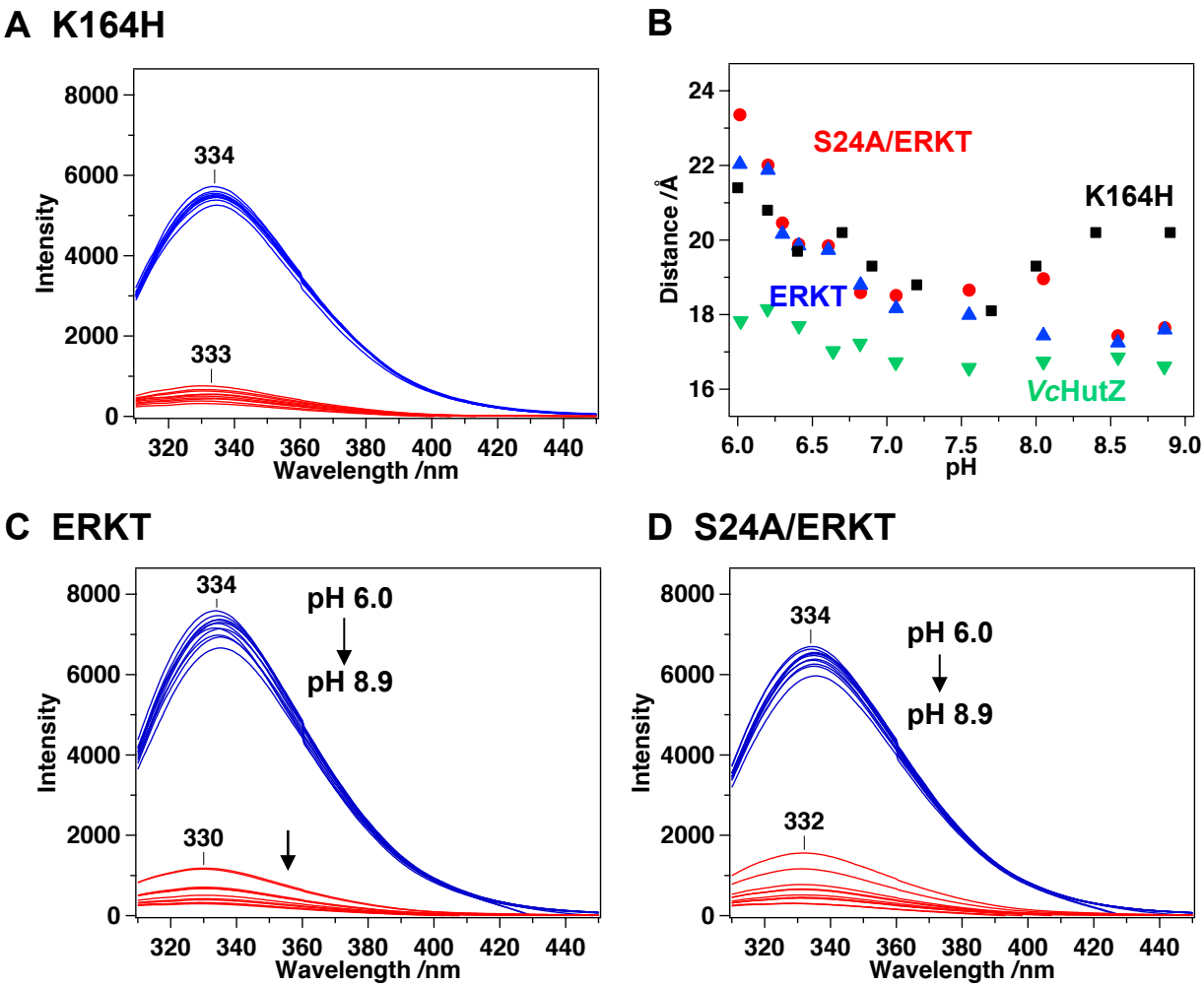

Fig. 7. Fluorescence spectra. Fluorescence spectra of heme-K164H, heme-ERKT, and heme-S24A/ERKT Alr5027 mutants. (A–C) Fluorescence spectra of K164H (A), ERKT (B) and S24A/ERKT (C) mutants in the absence (red lines) and presence (blue lines) of heme. Spectra were recorded at pH 6.0, 6.2, 6.3, 6.4, 6.6, 6.8, 7.0, 7.5, 8.0, 8.5 and 8.8, with excitation at 295 nm. The sample concentration was 5 μM. (D) pH dependence of the distance between heme and Trp103 in K164H, ERKT, and S24A/ERKT mutants.

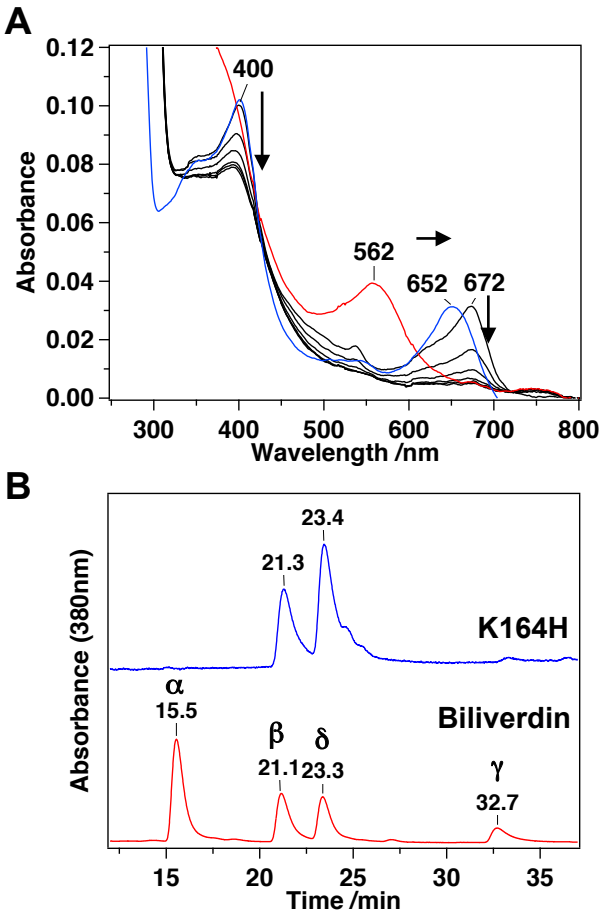

Fig. 8. Heme degradation of the K164H mutant using H_2O_2 and ascorbic acid. (A) Reaction of the verdoheme-K164H mutant with 1 mM ascorbic acid at pH 8.0. Absorption spectra in the reaction with ascorbic acid after the formation of verdoheme (blue line) by addition of 0.1 mM H_2O_2. Spectra were recorded before and after the addition of ascorbic acid at 4, 8, 16, 24, and 32 min (black line). Ferrozine (0.10 mM) was added 32 min after the reaction (green line). (B) HPLC chromatograms of biliverdin standard (red line) and final products of the heme-K164H mutant (blue line) monitored at 380 nm.

Supplementary Information

A single mutation converts Alr5027 from cyanobacteria *Nostoc* sp. PCC 7120 to a heme-binding protein with heme-degrading ability

Nobuhiko Dojun[a], Kazuyoshi Muranishi[a], Koichiro Ishimori[a.b], and Takeshi Uchida[a,b,*]

[a] Graduate School of Chemical Sciences and Engineering, Hokkaido University, Sapporo 060-8628, Japan

[b] Department of Chemistry, Faculty of Science, Hokkaido University, Sapporo 060-0810, Japan

*****Corresponding author at Department of Chemistry, Faculty of Science, Hokkaido University, Sapporo 060-0810, Japan.

E-mail address: uchida@sci.hokudai.ac.jp, Phone: +81-11-706-3501 (T. Uchida).

Table S1. Primer used for construction of expression vectors for mutants.

Constructs	Sequence (up sense; bottom, anti-sense)
K164H_F	GGTGACCATGGCTGAAAGCTTGCGGCC
K164H_R	TCAGCCATGGTCACCGGTAATCGGAAC
D163H_F	ACCGGTCATAAAGGCTGAAAGCTTGCG
D163H_R	GCCTTTATGACCGGTAATCGGAACCAG
G165H_F	GACAAACATTGAAAGCTTGCGGCCGCA
G165H_R	CTTTCAATGTTTGTCACCGGTAATCGG
G165HG_F	GACAAACATGGCTGAAAGCTTGCGCC
G165HG_R	TCAGCCATGTTTGTCACCGGTAATCGG
CTE_F	CATCGTAAGATTTCTAAAGGCTGAAAGCTTGCG
CTE_R	AGAAATCTTACGATGGTCACCGGTAATCGGAAC
ERKT_F	CAGAACGGAAAACCGCGATCATTTCGACGATT
ERKT_R	CGGTTTTCCGTTCTGACTGAAACTCCTGAATGA
S24A/ERKT_F	ATCATTGCGACGATTAGCGAACAAGGG
S24A/ERKT_R	AATCGTCGCAATGATCGCCCTTTTCCG

F indicates the forward direction primer, and R indicates the reverse direction primer. The underlined based signify the introduced mutations.

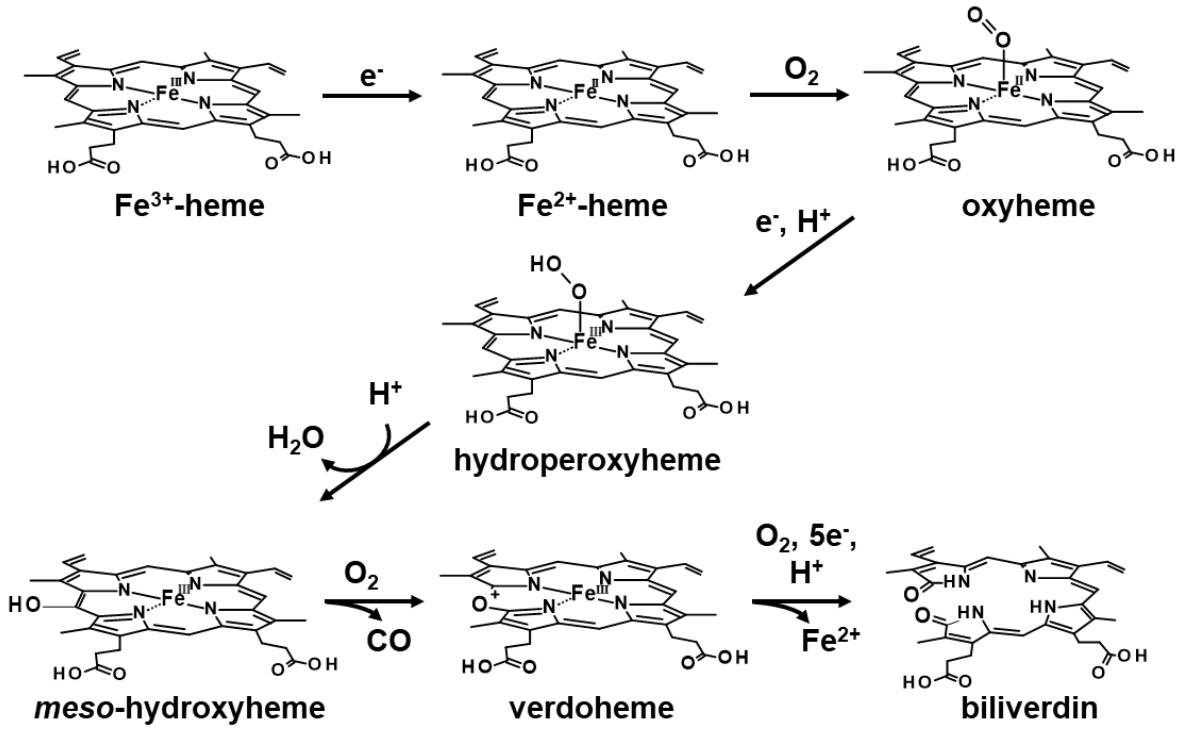

Fig S1. Heme-degradation mechanism of HutZ.

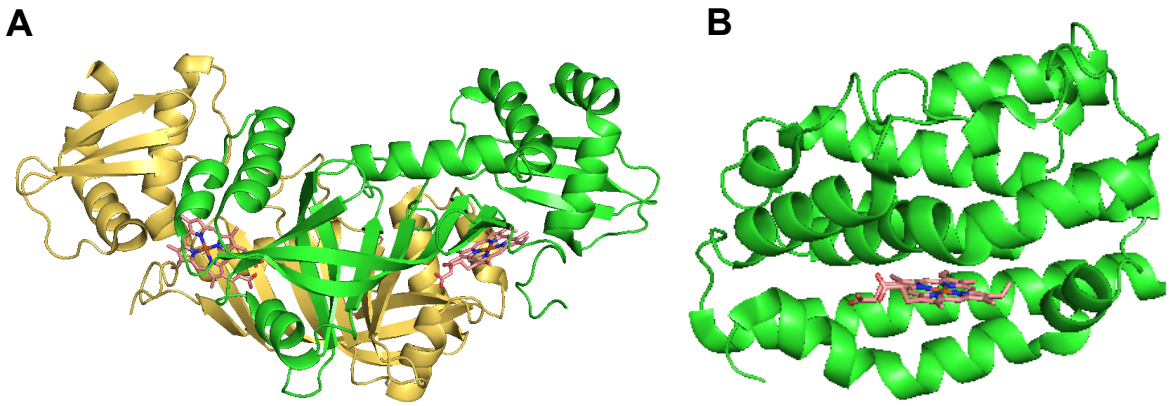

Fig S2. Crystal structure of (A) HugZ from *Helicobacter pylori* (PDB ID 3GAS) and (B) rat HO-1 (PDP ID 4G7L). HutZ is a dimer, whereas HO-1 is a monomer.

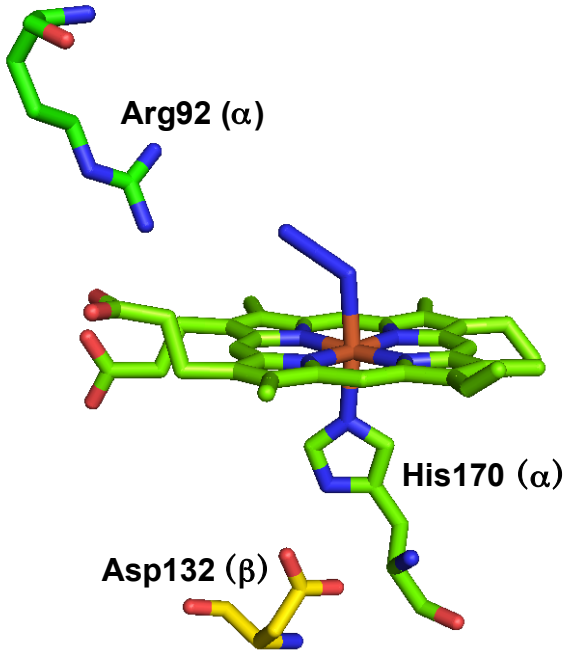

Fig S3. Putative active site of the *Vc*HutZ homologous protein, HugZ, from *H. pylori* (PDB ID 3GAS). Residue numbering is based on *Vc*HutZ

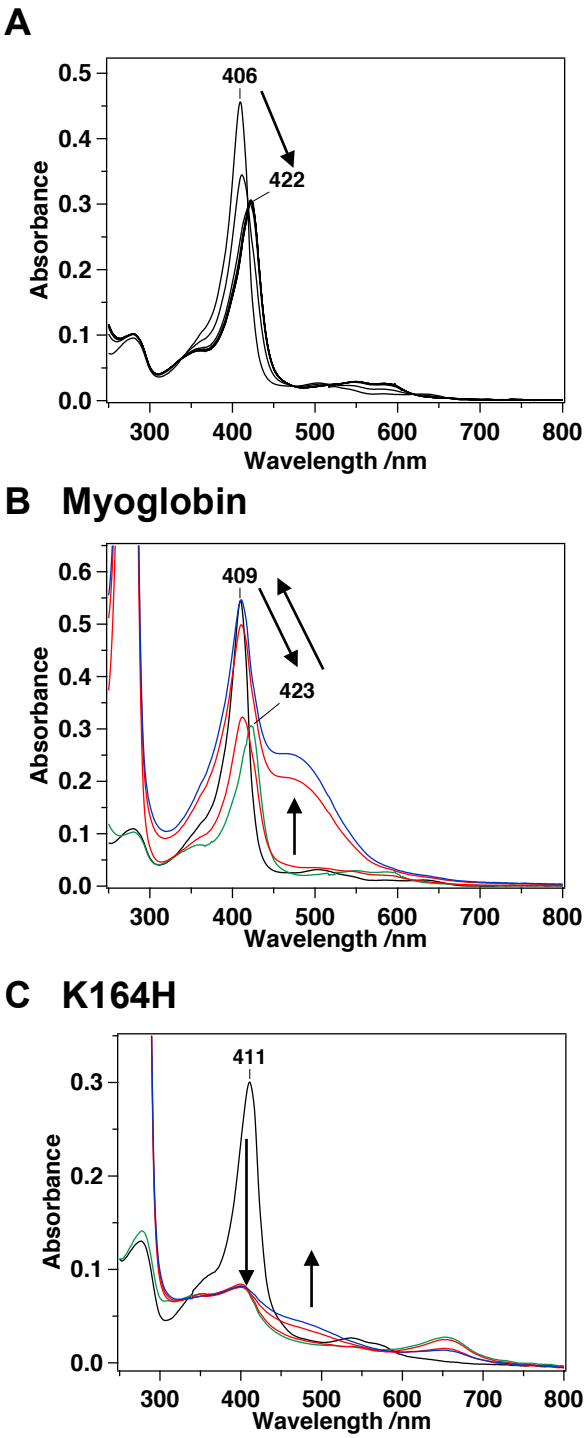

Fig S4. (A) Absorption spectra of myoglobin in a reaction containing 0.1 mM H_2O_2 at pH 8.0. Spectra were measured before the addition of H_2O_2, and at 1-min intervals for 10 min after the addition of H_2O_2. (B, C) Reaction of myoglobin (B) and heme-K164H mutant (C) with H_2O_2 (90 μM) in the presence of 0.45 mM guaiacol at pH 8.0. The absorption spectrum before the reaction is shown as a black line. The reaction with guaiacol was monitored before mixing (green line), and 1, 20 (red lines), and 30 min (blue line) after mixing.

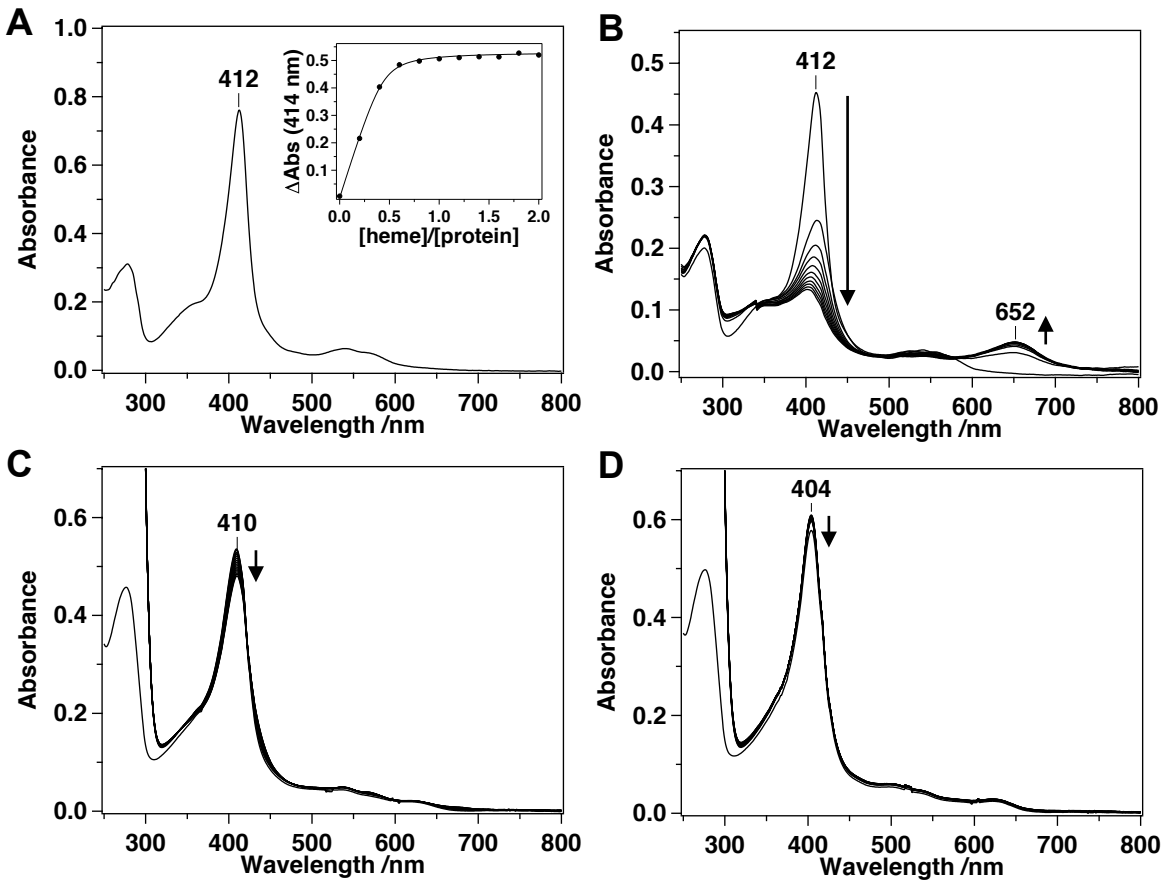

Fig. S5. Absorption spectrum of the heme-CTE mutant**.** (A) Absorption spectrum of the heme-CTE mutant. The inset shows differences at 414 nm. (B) Heme-degradation reaction of the CTE mutant with H_2O_2 (0.1 mM) at pH 8.0. The reaction conditions in (A) and (B) were same as those in Fig 6A and C, respectively. (C, D) Heme-degradation reaction of the CTE mutant with 1.0 mM ascorbic acid at pH 8.0 (C) and pH 6.0 (D). Spectra were recorded before addition of ascorbic acid, and at 2-min intervals for 30 min after addition of ascorbic acid.

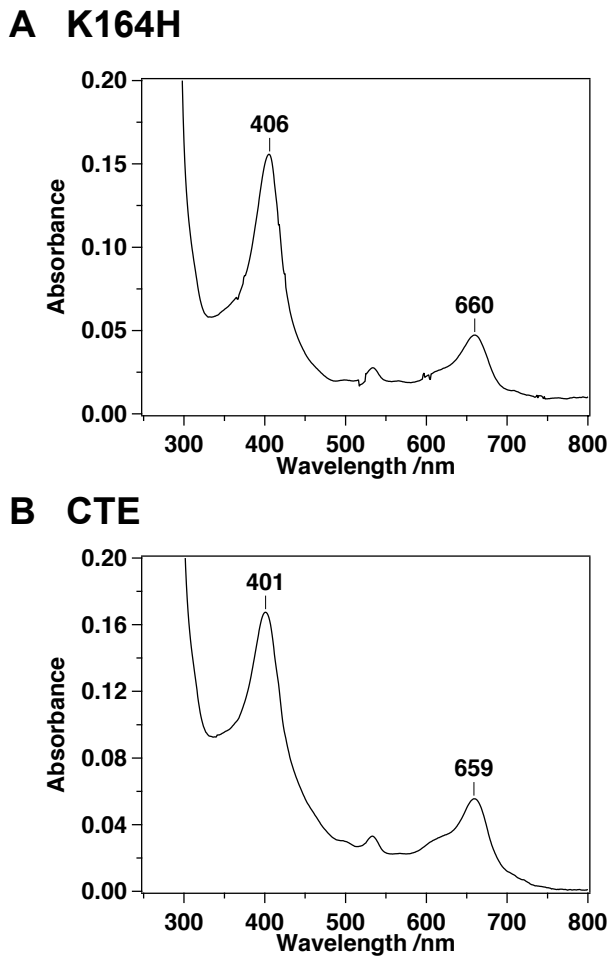

Fig S6. Absorption spectra of verdoheme in aqueous pyridine. (A) K164H and (B) CTE heme-bound mutants were reacted with H_2O_2 under the same conditions at those in Figure 5. Pyridine (final concentration, 33%) was added to the reaction mixture 10 min after the reaction to liberate the product from the protein.

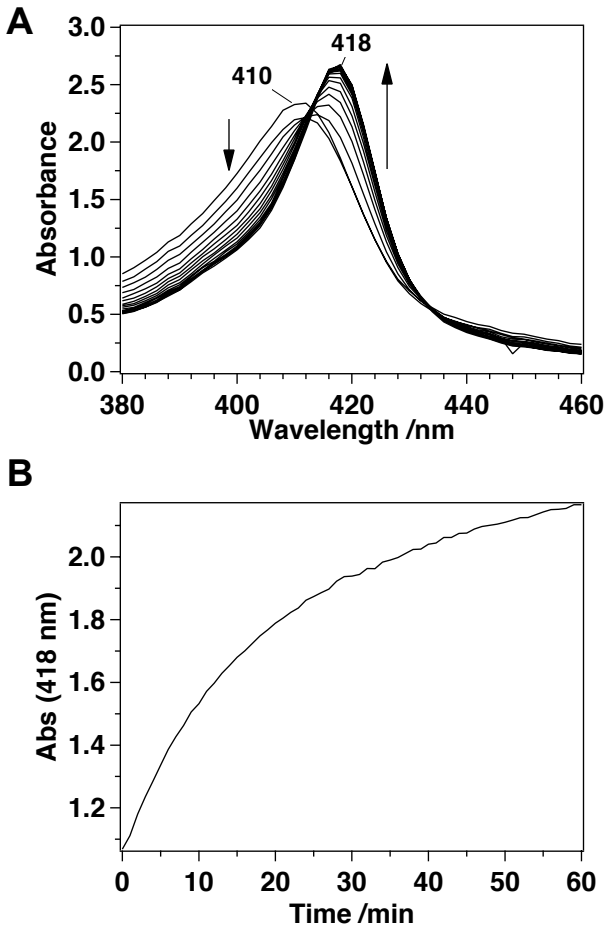

Fig. S7. Determination of the reduction rate of heme. (A) Absorption spectra of heme-K164H after the addition of 1 mM ascorbic acid at pH 8.0 under a CO atmosphere. (B) Time course of absorbance changes at 418 nm.

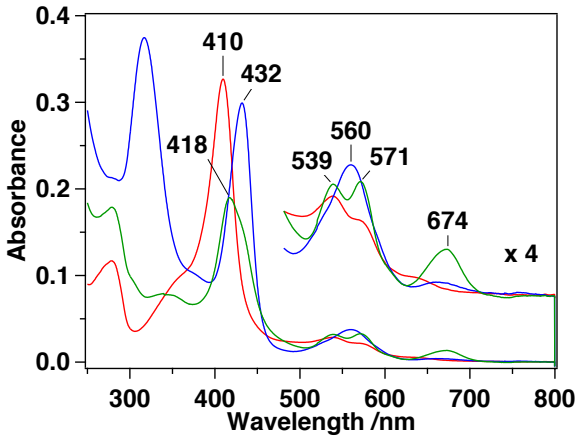

Fig. S8. Absorption spectrum of the heme-K164H mutant**.** Ferric form (red), ferrous form (blue), reduced by sodium dithionite (0.2 mM), oxyferrous from, produced by air to ferrous form (green). The samples were in 50 mM Tris-HCl and 150 mM NaCl (pH 8.0). Although 1 μM catalase was involved in the solution to decompose H_2O_2 produced by reduction of contaminated molecular oxygen by dithionite, the spectra of catalase was subtracted from each spectrum.

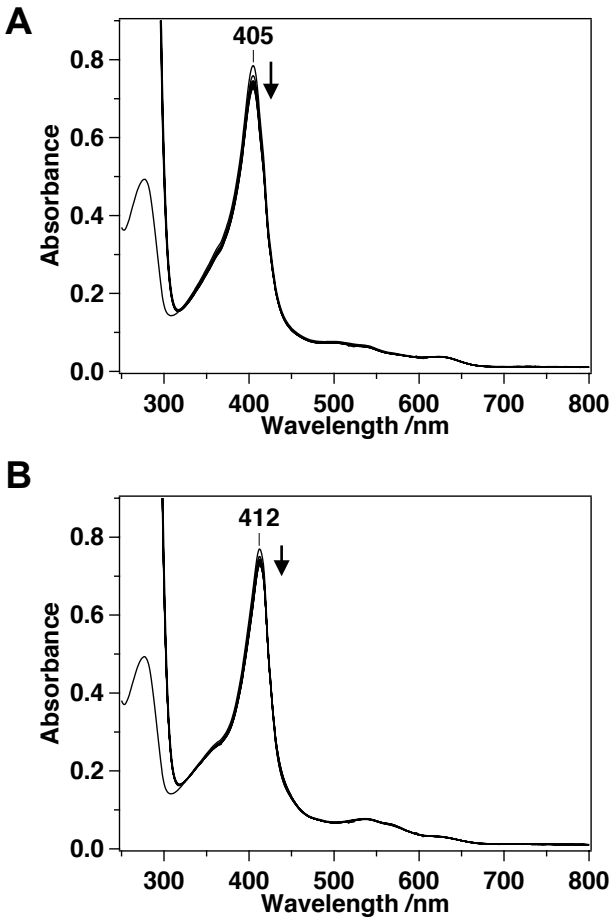

Fig. S9. Absorption spectrum of the heme-ERKT mutant. Heme-degradation reaction of the heme-Alr5027 ERKT mutant with ascorbic acid at pH 6.0 (A) and pH 8.0 (B). Spectra were monitored before the addition of ascorbic acid, and at 2-min intervals for 30 min after the addition of ascorbic acid.

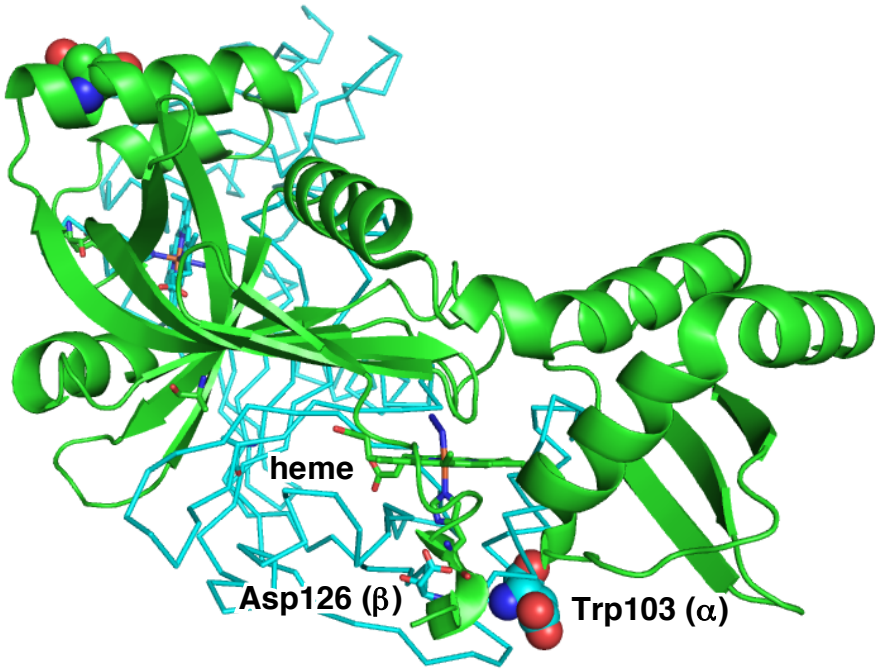

Fig S10. Location of Trp103 and heme on the HugZ crystal structure (PBD 3GAS). Residues are numbered according to the amino acid sequence of Alr5027 from cyanobacteria *Nostoc sp*. PCC7120. Green and cyan show each protomer. Trp103 is present in a different protomer (green) from that (cyan) containing the nearby Asp126 in a different subunit.

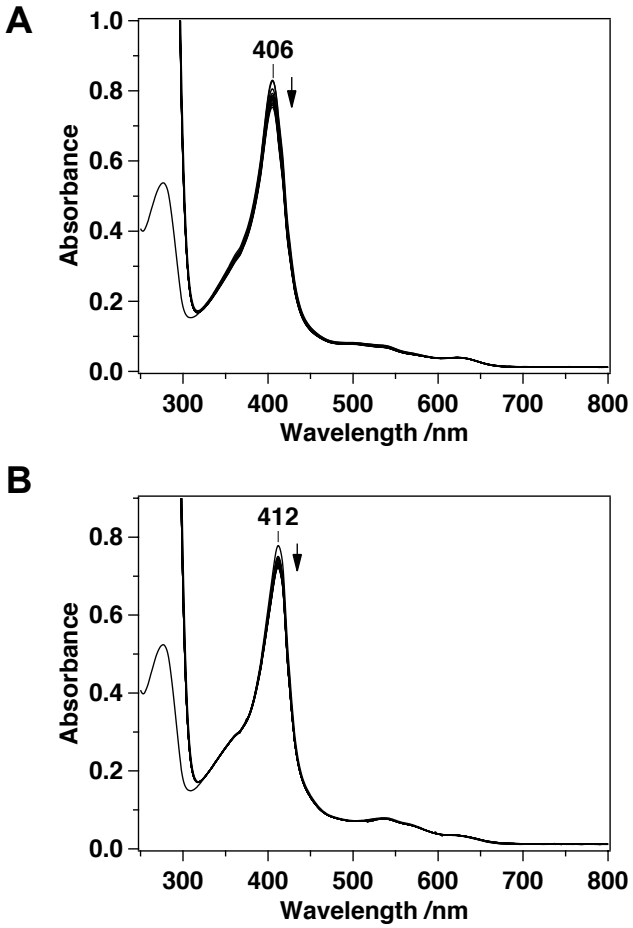

Fig. S11. Heme-degradation reaction of the heme-Alr5027 S24A/ERKT mutant with ascorbic acid at pH 8.0 (A) and pH 6.0 (B). Spectra were monitored before the addition of ascorbic acid, and at 2-min intervals for 30 min after the addition of ascorbic acid.